Current plate movements across the Mid-Atlantic Ridge determined from 5 years of continuous GPS measurements in Iceland

Halldór Geirsson,[1] Thóra Árnadóttir,[2] Christof Völksen,[3] Weiping Jiang,[2,4] Erik Sturkell,[2] Thierry Villemin,[5] Páll Einarsson,[6] Freysteinn Sigmundsson,[2] and Ragnar Stefánsson[1,7]

Received 4 March 2005; revised 11 May 2006; accepted 30 June 2006; published 28 September 2006.

[1] We analyze data spanning up to 5 years from 18 continuous GPS stations in Iceland, computing daily positions of the stations with three different high-level geodetic processing software packages. We observe large-scale crustal deformation due to plate spreading across Iceland. The observed plate divergence between the North American and the Eurasian plates is in general agreement with existing models of plate motion. Spreading is taken up within a ~100–150 km wide plate boundary zone that runs through the island. Of the two parallel branches of the plate boundary in south Iceland, the eastern volcanic zone is currently taking up the majority of the spreading and little is left for the western volcanic zone. The plate boundary deformation field has been locally and temporarily affected in south Iceland by two M_w = 6.5 earthquakes in June 2000, inflation at Katla volcano during 2000 to 2004, and an eruption of Hekla volcano in February 2000. All stations with significant vertical velocities are moving up relative to the reference station REYK, with the highest velocity exceeding 20 mm/yr in the center of the island.

Citation: Geirsson, H., T. Árnadóttir, C. Völksen, W. Jiang, E. Sturkell, T. Villemin, P. Einarsson, F. Sigmundsson, and R. Stefánsson (2006), Current plate movements across the Mid-Atlantic Ridge determined from 5 years of continuous GPS measurements in Iceland, *J. Geophys. Res.*, *111*, B09407, doi:10.1029/2005JB003717.

1. Introduction

[2] The tectonic setting of Iceland on the divergent Mid-Atlantic Ridge, with frequent earthquakes and volcanic eruptions, makes it an ideal setting for studying crustal deformation. Various techniques have been used for this purpose in Iceland. Frequent GPS campaign measurements have been conducted since 1986 [*Foulger et al.*, 1986], providing a wealth of information on plate movements, seismic, and volcanic processes [e.g., *Jónsson et al.*, 1997; *Hreinsdóttir et al.*, 2001; *Árnadóttir et al.*, 2001; *Sturkell et al.*, 2003a]. Previous studies have focused on parts of the plate boundary, allowing good spatial coverage of limited areas. However, temporal resolution has been limited due to the intermittent nature of campaign GPS measurements. Continuous GPS measurements (CGPS) provide enhanced temporal resolution and allow much improved estimation of station velocities, compared to campaign GPS. The first CGPS station in Iceland was installed in Reykjavík (REYK) in 1995 and presently there are 18 permanent GPS sites in Iceland, of which 14 belong to the ISGPS network (Figure 1). The primary aims of the ISGPS network are to monitor crustal deformation processes in near real time and to contribute to better understanding of processes causing crustal deformation and natural hazards in Iceland.

[3] Iceland is spreading at a full rate ranging from 18.9 mm/yr at the plate boundary in north Iceland to 20.2 mm/yr at the Reykjanes ridge SW of Iceland (Figure 1), according to the REVEL plate motion model [*Sella et al.*, 2002]. Iceland owes its existence to excessive magmatism caused by the North Atlantic mantle plume, currently centered beneath the Vatnajökull ice cap (Figure 1). The Mid-Atlantic plate boundary comes onshore on the Reykjanes Peninsula in south Iceland and continues east along the peninsula toward the Hengill triple junction area. At Hengill the plate boundary splits in two directions: NNE along the western volcanic zone and toward east along the south Iceland seismic zone (SISZ), which is an E-W transform fracture zone. The south Iceland seismic zone merges with a propagating rift zone, the eastern volcanic zone, which continues north through the country. It is offset again at the Tjörnes fracture zone (TFZ) toward the Kolbeinsey ridge. The plate boundary rifting is more complicated in south Iceland than in the north. Plate divergence in south Iceland is divided between two parallel rift zones, the eastern and western volcanic zones. Previous studies have suggested that rifting is pres-

[1]Icelandic Meteorological Office, Reykjavík, Iceland.
[2]Nordic Volcanological Center, Institute of Earth Sciences, University of Iceland, Reykjavík, Iceland.
[3]Bavarian Academy of Sciences and Humanities, Munich, Germany.
[4]Now at GPS Research Center, Wuhan University, Wuhan, China.
[5]Laboratoire de Géodynamique des Chaînes Alpines, Université de Savoie, Le Bourget du Lac, France.
[6]Institute of Earth Sciences, University of Iceland, Reykjavík, Iceland.
[7]Now at Faculty of Natural Resource Science, University of Akureyri, Akureyri, Iceland.

0148-0227/06/2005JB003717$09.00

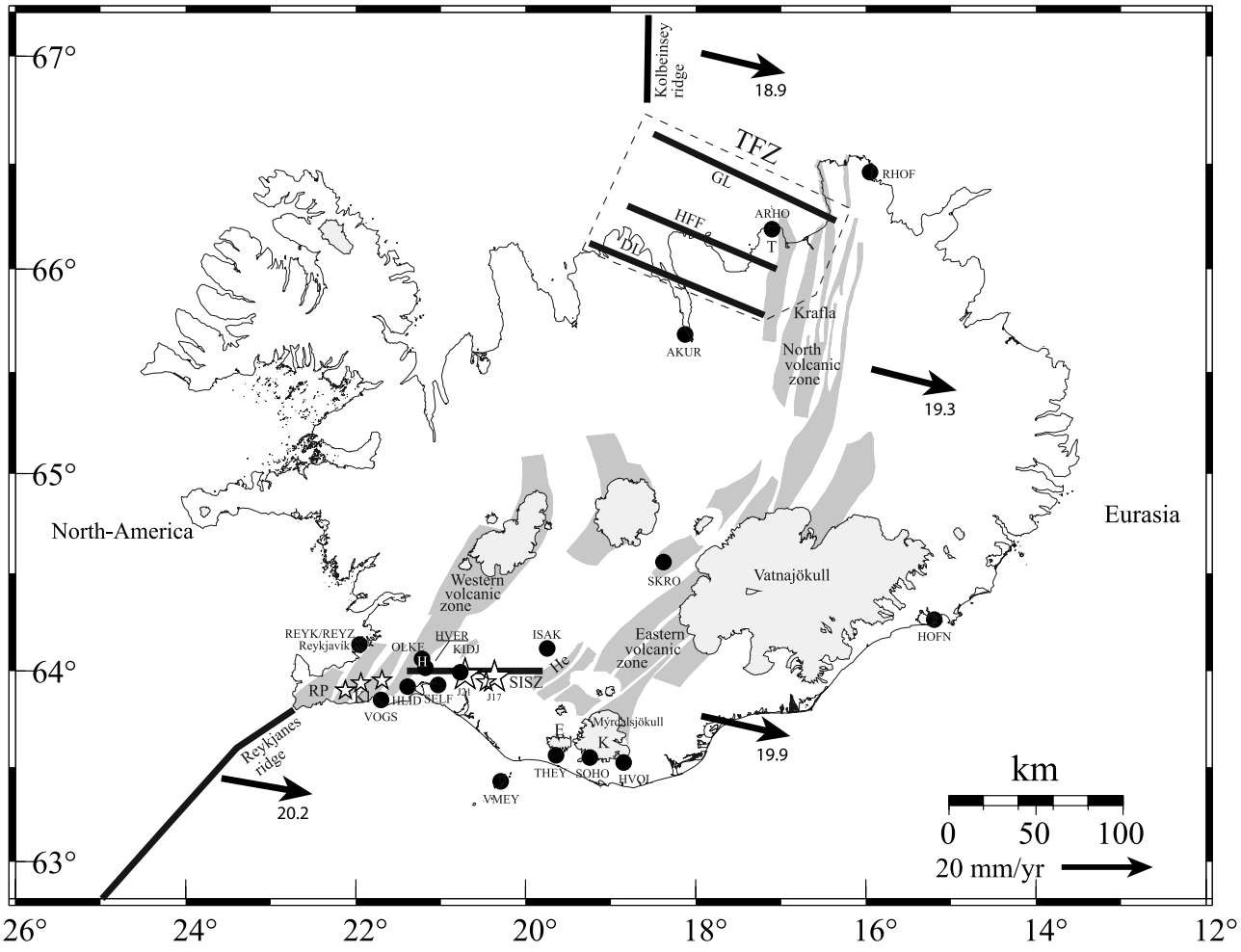

Figure 1. Schematic overview of the plate boundary in Iceland. Arrows show velocity vectors predicted by the REVEL plate motion model, relative to stable North America [*Sella et al.*, 2002]. The transform zones and offshore ridge segments are schematically drawn with black heavy lines. Dark gray areas are active fissure swarms [*Einarsson and Saemundsson*, 1987], and light gray areas outline glaciers. Continuous GPS stations are shown with black dots. Stars note $M > 5$ earthquake epicenters on 17 and 21 June 2000. Abbreviations on map: RP, Reykjanes Peninsula; Kl, Kleifarvatn; H, Hengill volcano; SISZ, south Iceland seismic zone; He, Hekla volcano; K, Katla volcano; E, Eyjafjallajökull volcano; T, Tjörnes Peninsula; TFZ, Tjörnes fracture zone (outlined with black dashed lines); GL, Grímsey lineament; HFF, Húsavík-Flatey fault, DL, Dalvík lineament [after *Rögnvaldsson et al.*, 1998].

ently mostly taken up by the eastern volcanic zone [*Sigmundsson et al.*, 1995; *LaFemina et al.*, 2005].

[4] The transform zones, the south Iceland seismic zone and the Tjörnes fracture zone are the most active seismic zones of Iceland, where the largest earthquakes occur. The SISZ is approximately 70 km long (E-W) and about 20 km wide (N-S) (Figure 1). It accommodates the relative plate motion along an array of N-S trending right-lateral strike-slip faults in a ''bookshelf faulting'' mode instead of a single E-W trending left-lateral fault [*Einarsson and Eiríksson*, 1982; *Sigmundsson et al.*, 1995]. Destructive earthquake sequences have occurred during historic times in the SISZ at intervals of 45 to 112 years [*Einarsson et al.*, 1981]. The earthquake sequences usually consist of several earthquakes with M > 6 that occur on N-S trending strike-slip faults. Such a sequence occurred in June 2000 with two M_w = 6.5 earthquakes spaced 17 km and 3.5 days apart [*Árnadóttir et al.*, 2001; *Pedersen et al.* 2001; *Stefánsson et al.*, 2003; *Clifton and Einarsson*, 2005]. The former earthquake, on 17 June, triggered earthquake activity toward west, including three $M_w > 5$ events on the Reykjanes Peninsula [*Pagli et al.*, 2003; *Clifton et al.*, 2003; *Árnadóttir et al.*, 2004]. The continuous GPS sites captured deformation due to these events, although the station coverage was limited in 2000.

[5] The Tjörnes fracture zone in north Iceland is a transform zone, like the south Iceland seismic zone, that connects the northern volcanic zone to Kolbeinsey ridge (Figure 1). The structure is mostly offshore. Instead of a single seismic zone like the SISZ, the TFZ is composed of three nearly parallel seismic lineaments: the Húsavík-Flatey fault, the Grímsey lineament, and the Dalvík lineament [*Rögnvaldsson et al.*, 1998] (Figure 1). Currently, the Grímsey lineament is the most seismically active of the

three. As in the SISZ, earthquakes with M > 6 occur in the TFZ, the most recent being a M = 6.4 event in 1976 at the SE tip of the Grímsey lineament [*Einarsson*, 1987]. Continuous GPS measurements indicate the amount of spreading taken up by each of the three lineaments and they help in monitoring any temporal variations that may occur in relation to seismic activity.

[6] Magmatic activity is frequent in Iceland, with one eruption on average every few years. Continuous GPS is a powerful tool to monitor volcanoes as the data processing can be done in near real time using predicted satellite orbits. One of Iceland's most threatening volcanoes, Katla, is a subglacial volcano in south Iceland. Its last large eruption was in 1918, but seismic tremors related to minor volcanic activity were recorded in 1955 and 1999. Since 1999, Katla has been showng signs of increased unrest, manifested in high seismicity, increased geothermal activity, and deformation observed at the continuous GPS stations SOHO and HVOL as well as at campaign GPS sites.

[7] This study reports initial results from the permanent GPS network in Iceland from 18 March 1999 to 18 March 2004. The time series show secular motion due to plate spreading as well as temporal variations of deformation fields associated with two M_w = 6.5 earthquakes, volcanic unrest at Katla, and an eruption of the Hekla volcano. Vertical rates suggest the center of Iceland is currently rising by about 20 mm/yr with respect to coastal areas.

2. ISGPS Network and Data Processing

2.1. Network Description

[8] Continuous GPS measurements in Iceland began in November 1995 when the station REYK was installed by the Bundesamt für Kartographie und Geodäsie (BKG, formerly IfAG), Germany (Figure 1). In May 1997 a second station, HOFN, was installed at Höfn, Hornafjördur, by BKG and LMI (National Land Survey of Iceland). In September 1998 the third station, REYZ, was installed by the same groups a few meters from REYK. REYZ is a combined GPS/GLONASS station.

[9] Seismic and volcanic unrest led to the installation of the next set of stations. Intensive seismicity in the Hengill area, associated with uplift at a rate of 20 mm/yr between 1994 and 1998 [*Sigmundsson et al.*, 1997; *Feigl et al.*, 2000] caused public concern, motivating the initiation of the ISGPS network. The ISGPS network is a cooperative project between the Icelandic Meteorological Office, the Nordic Volcanological Center, the Science Institute, the University of Iceland, and the University of Savoie, France. The first ISGPS station was installed at VOGS on 18 March 1999, and three more stations were installed in the Hengill area (OLKE, HVER, and HLID) in March to May 1999 (Figure 1). Although the uplift and intensive seismicity in the Hengill area ceased in early 1999, these stations have been operated continuously since their installation.

[10] Seismic unrest at Katla and Eyjafjallajökull volcanoes accompanied by a small flood in July 1999 from Mýrdalsjökull glacier [*Sturkell et al.*, 2003b; *Sigurdsson et al.*, 2000] led to the installation of three stations: SOHO (September 1999), HVOL (October 1999), and THEY (May 2000), located at the southern slopes of these volcanoes. Station VMEY (Figure 2) was installed in July 2000 in the Westmann Islands, south of Iceland, to monitor possible magmatic movements at Heimaey, which last erupted in 1973. The damaging June 2000 earthquakes in south Iceland spurred installation of two new stations in the western part of the seismic zone (KIDJ in January 2001 and SELF in February 2002). The stations are located in its western part because earthquake sequences in the seismic zone tend to progress westward with time [*Einarsson et al.*, 1981]. Station ISAK (installed in January 2002) was funded by the National Power company to monitor volcanic activity at Hekla volcano, that erupted last in 1947, 1970, 1980, 1991, and 2000, and poses a threat to nearby power plants. Station SKRO, installed in September 2000, marked the beginning of cooperation with the University of Savoie which led to the installation of two more stations in Northern Iceland (RHOF in July 2001 and ARHO in June 2002). Station AKUR, operated by the National Land Survey of Iceland, started recording in July 2001.

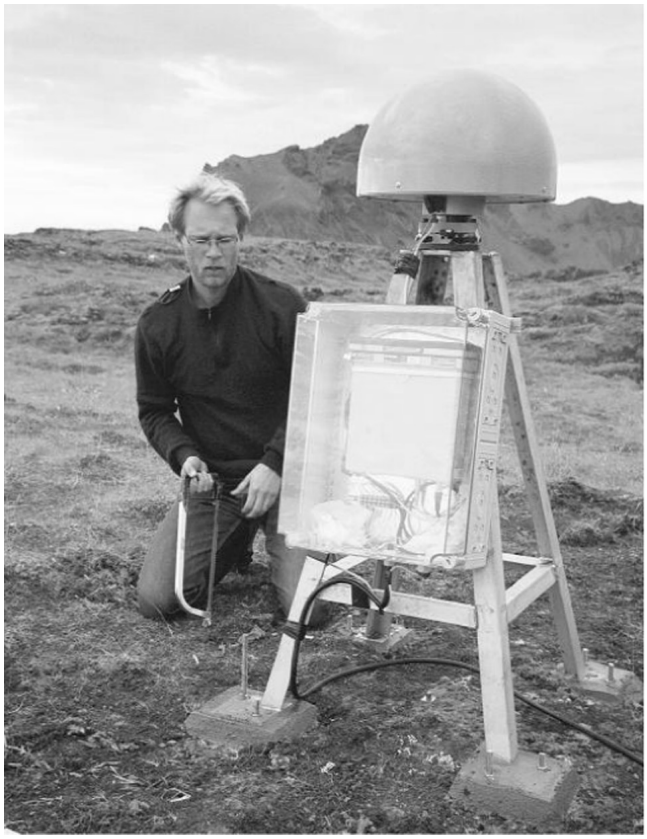

Figure 2. A photo from station VMEY, showing the monumentation used for the ISGPS network. The choke ring antenna is mounted on a steel quadripod and covered with a SCIGN radome. The receiver is in a plastic box on the side of the quadripod.

[11] The ISGPS monument is kept as simple and robust as possible and consists of a 1-m-high stainless steel quadripod bolted into solid bedrock (Figure 2). The actual physical point being measured is a classic geodetic copper benchmark cemented into solid bedrock or a concrete platform. The quadripod is leveled and centered over the benchmark and the antenna is fastened to the top of the quadripod. Choke ring antennas and plastic hemispherical radomes

from Southern California Integrated GPS Network (SCIGN) are used at all ISGPS sites. At REYK and HOFN a choke ring antenna without a radome is currently used. Before 21 September 2001 a Trimble groundplane antenna with a radome (TRM22020.00+GP DOME) was used at HOFN. At REYZ a conical Ashtech radome is used.

2.2. Data Processing

[12] Dual-frequency phase and pseudorange data are recorded at all ISGPS sites at 15-s intervals in the internal memory of the receivers in 24-hour-long files. Elevation angle limit varies from 5° to 15° between sites, depending on the local terrain. Data files are downloaded automatically on a daily basis via a modem-to-modem connection during night hours. After data have been downloaded from the receivers, preliminary results (coordinates) are automatically calculated using predicted satellite orbits from the Center of Orbit Determination in Europe (CODE) and Bernese V4.2 software [*Hugentobler et al.*, 2001]. Results are automatically posted on the ISGPS web pages (http://www.vedur.is) that are used for near real-time monitoring of crustal deformation. Later the data are reprocessed using CODE final orbits.

[13] The data have also been analyzed with GIPSY/OASIS II [*Webb and Zumberge*, 1993] and GAMIT/GLOBK [*King and Bock*, 2003; *Herring*, 2003a]. The largest differences between the different processing schemes is that the Bernese strategy depends upon a single reference station, whereas GAMIT/GLOBK uses a number of fidicual stations to tie the results to the International Terrestrial Reference Frame (ITRF) 2000 [*Altamimi et al.*, 2002], and GIPSY/OASIS II uses the precise point positioning method of GIPSY/OASIS II to estimate coordinates in the ITRF2000 reference frame without using data from fiducial stations.

2.2.1. Bernese 4.2

[14] When analyzing data with the Bernese software, we used a processing sequence described by *Árnadóttir et al.* [2000] that includes (1) cycle slip screening and outlier removal using ionosphere-free linear combination (L3) double-difference phase residuals; (2) estimation of an ionospheric model using the geometry-free linear combination (L4); (3) using the previously obtained ionospheric model and constraining the coordinates of REYK the L1 and L2 ambiguities were estimated and saved using the quasi-ionosphere-free (QIF) ambiguity resolution strategy; 4) introducing the L1 and L2 ambiguities the L3 linear combination was used to calculate the final station coordinates and full covariance matrix. In this run we tightly constrained (effectively fixed) our reference station, REYK, at its ITRF97 [*Boucher et al.*, 1999] coordinates.

2.2.2. GIPSY/OASIS II

[15] While the Bernese software is based on parameter elimination using the double-difference technique, GIPSY/OASIS II processes undifferenced observation [*Webb and Zumberge*, 1993]. Therefore common parameters such as the clock parameters of the GPS satellites and receivers have to be estimated in GIPSY/OASIS II, which are eliminated by the double-difference technique used by the Bernese and GAMIT/GLOBK softwares. In principle, however, these two methods give the same results. GIPSY/OASIS II offers one special processing strategy that is called precise point positioning [*Zumberge et al.*, 1997]. We use precise satellite clock and orbit information supplied by the Jet Propulsion Laboratory (JPL). The advantage of the precise point positioning method is that it allows one to estimate absolute station coordinates in the ITRF2000 without using data from fiducial stations. Instead of fixing ambiguities, only float solutions using the L3 combination are computed, which are equivalent to fixed solutions when the observation window is longer than 8–12 hours [*Mervart*, 1995].

2.2.3. GAMIT/GLOBK

[16] We also analyzed the GPS data using the GAMIT/GLOBK software version 10.6 [*King and Bock*, 2003; *Herring*, 2003a] using the procedure described by *Árnadóttir et al.* [2006]. Precise satellite orbits and Earth rotation parameters from the International GPS Service (IGS) were used. We processed data from 22 global stations to realize the ITRF2000 reference frame for the station positions and velocities, using the stabilization procedure described by *McClusky et al.* [2000].

2.2.4. Comparison of Results From Different Processing Software

[17] The absolute motion of REYK in ITRF2000 using results from GIPSY/OASIS II processing and GAMIT/GLOBK is plotted in Figure 3. The time series show that the results from the two processing softwares agree well. Details of the time series are revealed in a similar manner in both softwares and the velocities do not differ significantly although we see a small difference in the trend of the vertical component.

[18] We transformed the ITRF2000 time series for the permanent stations in Iceland from GAMIT/GLOBK and GIPSY/OASIS II to a local east-north-up coordinate system, using REYK as the reference station in order to compare all three processing softwares. Figure 4 shows a comparison of the results from the different processing softwares, for the motion of VOGS relative to REYK (see also the auxiliary material).[1] The relative velocities for VOGS agree well and the phase and amplitudes of the annual signals are similar for all processing softwares, using REYK as the reference station. Coseismic offsets due to the June 2000 earthquake sequence are also similar. There is slightly higher noise in the GIPSY/OASIS II solution, especially in the east component, because ambiguities are not resolved in the GIPSY/OASIS II processing strategy. In the vertical component, offsets due to radome installation are most pronounced in the GAMIT/GLOBK and Bernese solutions, but indiscernible in the GIPSY/OASIS II solution. We found the SCIGN radomes to cause an apparent shift of about −20 mm in the height when installed (Bernese processing). This effect has also been observed by *Schmidt et al.* [2003] for L3 estimate of station height and they explain the effect in terms of lensing of waves inside the dome. Vertical offsets due to equipment changes at REYK in 2003, marked R1, R2, and R3 in Figure 4, are most pronounced in the GAMIT and Bernese solutions. Overall, we found that the results from the different softwares agree well for all stations.

2.3. Time Series Analysis

[19] In this section we analyze the time series results obtained from the Bernese processing. The daily coordinate

[1] Auxiliary materials are available in the HTML. doi:10.1029/2005JB003717.

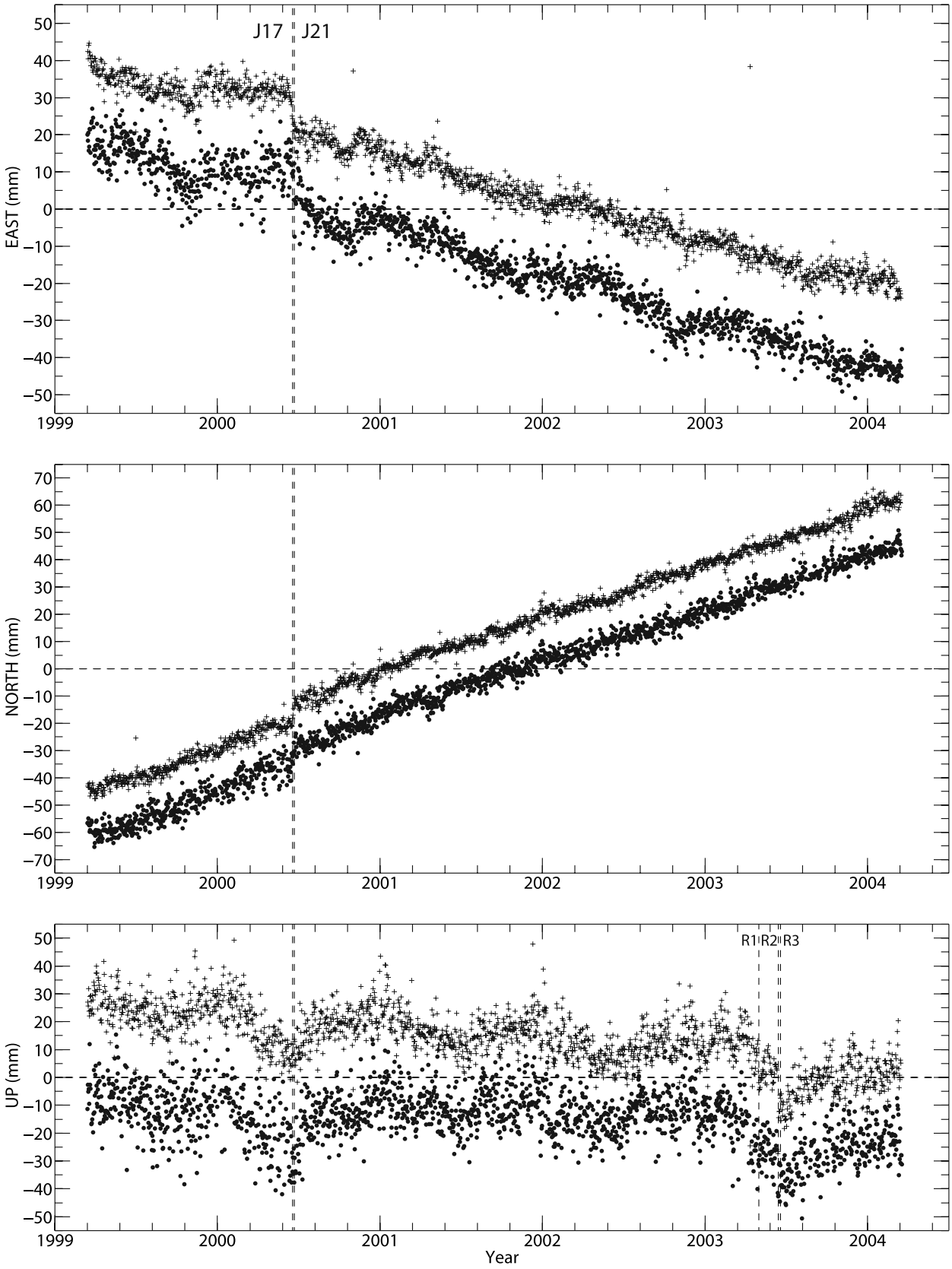

Figure 3. Time series of REYK from GAMIT/GLOBK (dots) and GIPSY/OASIS II (crosses) data processing in the ITRF2000. The time series are offset for clarity so that the GAMIT/GLOBK solution is always above the GIPSY/OASIS II solution. Vertical dashed lines indicate the times of the 17 and 21 June 2000 M_w = 6.5 earthquakes (J17 and J21) and times of equipment changes at REYK (R1, R2, and R3).

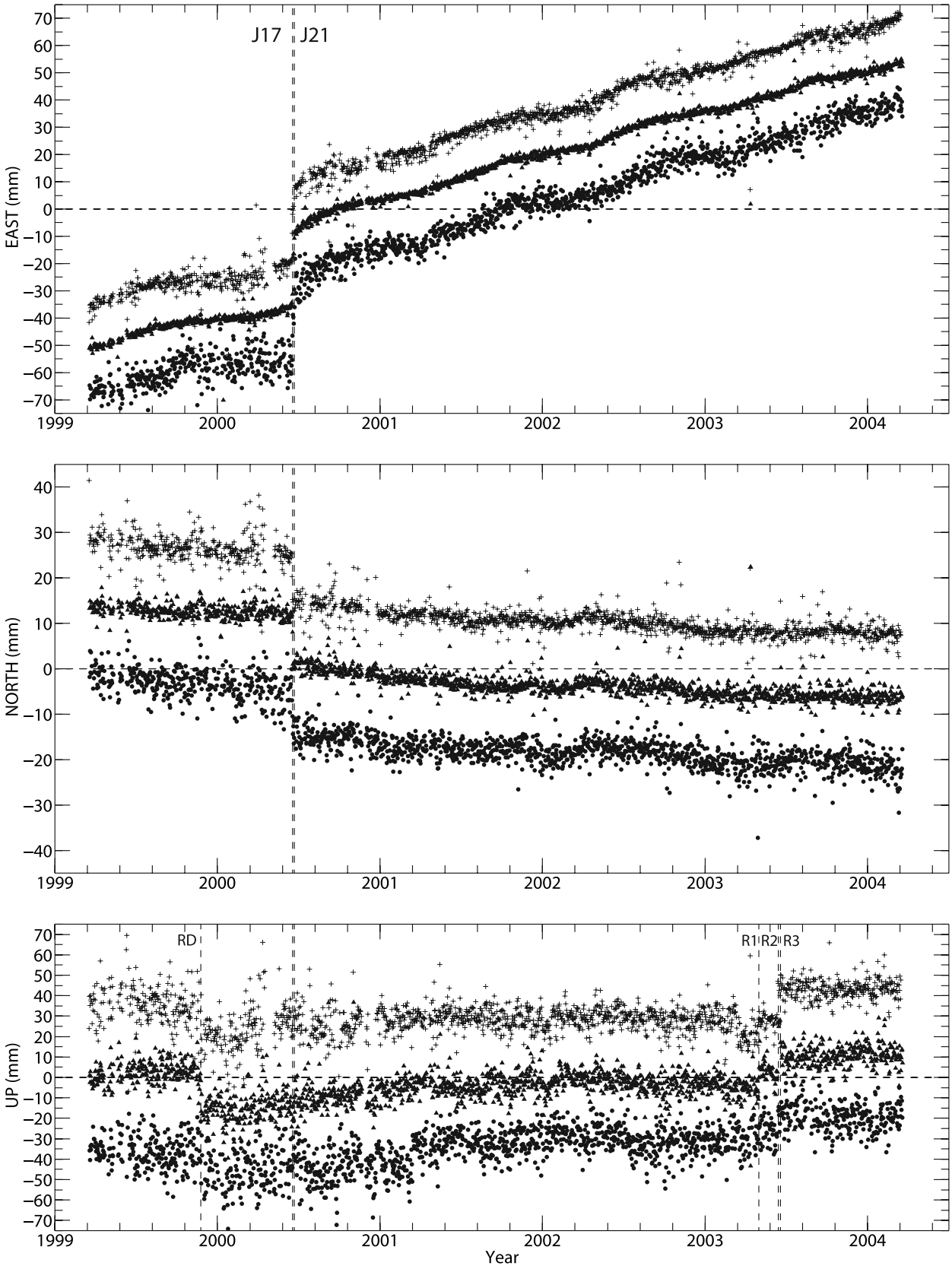

Figure 4. Time series for VOGS relative to REYK showing solutions from GAMIT/GLOBK (crosses), Bernese (triangles), and GIPSY/OASIS II (dots). The time series are offset so that the GAMIT/GLOBK solutions are on top, the Bernese solutions in the middle, and the GIPSY/OASIS II solutions below. Vertical dashed lines indicate the times of the 17 and 21 June 2000 M_w = 6.5 earthquakes (J17 and J21), the time of radome installation (RD) and times of equipment changes at REYK (R1, R2, and R3).

results from the Bernese processing were transformed from a geocentric XYZ to a local east-north-up coordinate system and displacements calculated relative to REYK being held fixed to build up the time series for all stations (Figure 5). We calculate the station velocities and annual sinusodial amplitudes and phases from the time series using a standard weighted least squares approach from

$$y(t) = a + bt + A\cos(2\pi t + \phi), \quad (1)$$

where $y(t)$ are the time series values at time t, $a + bt$ is a straight line component representing a constant velocity term and the cosine term models annual oscillations. The parameters estimated were a, b, A, and ϕ (Tables 1 and 2). We do not tabulate the offset parameter a, as it has no physical importance.

[20] In Figure 6 we added a constant velocity of −10.5 mm/yr and 1.6 mm/yr in the east and north components respectively to the station velocities to emphasize the plate spreading for visualization. The velocity shift was obtained from the REVEL model [*Sella et al.*, 2002] by assuming that the predicted velocities at REYK and HOFN are equal in magnitude, but in opposite directions. The daily coordinate uncertainty is taken as the square root of the diagonal elements in the daily solution covariance matrix. We refer to this uncertainty as the ''formal coordinate uncertainty''. The off-diagonal elements in the full covariance matrix are disregarded.

[21] The formal coordinate uncertainties are underestimated by the Bernese processing software [*Hugentobler et al.*, 2001] and need to be scaled to obtain a more rigorous estimate of the daily coordinate uncertainties. Moreover, the size of the formal coordinate uncertainty varies between different processing schemes within the Bernese software by at least a factor of 2. A more realistic estimate was found by scaling the formal uncertainties by equating their median values to the standard deviation of the residual time series from equation (1). The scale factors for the formal uncertainties were estimated to be 6 for the east component, 5 for the north component, and 3 for the vertical component.

[22] Outliers were defined as (1) data points with uncertainties larger than 3 times the median uncertainty for the corresponding component and station and (2) data points that deviate more than 4 times the scaled uncertainty from the residual of the model fit in equation (1). On average, 4% of the data points were rejected as outliers using this method.

[23] Before fitting the data, we removed all offsets in the time series. We corrected for offsets of −20 mm for the radome installation [*Geirsson*, 2003] on occasions when the radome was installed after the station had been in operation for some time (HLID, HVER, OLKE, SOHO, and VOGS). We corrected for an offset of $[e, n, u] = [6, -2, 74]$ mm due to an antenna change at HOFN in September 2001. We found three instances of common vertical offsets for all stations that we could track to changes at the reference station REYK, marked R1, R2, and R3 in Figure 4. We corrected the time series at all stations for these vertical offsets (10 mm at 2003.3301, 25 mm at 2003.4500, and −15 mm at 2003.4640). We also estimated these offsets from the GIPSY/OASIS II and GAMIT/GLOBK time series and found the total offset to be similar. We estimated offsets due to the south Iceland seismic zone June 2000 earthquake sequence and the February 2000 Hekla eruption by differencing average coordinates of 10 days on either side of these events. The station HOFN was not operating during 8 to 16 June, so we used average coordinates for HOFN 2 weeks before the 17 June earthquake (days 152 to 158) when estimating the coseismic offsets for HOFN relative to REYK. The station HLID was not in operation for 4 months before the earthquakes and we solved for the coseismic offset at HLID simultaneously when estimating the velocities and annual terms (equation (1)). We did not observe any significant vertical offsets at any station at the 2σ level, associated with the June 2000 earthquakes and the Hekla eruption (Table 3) and thus do not apply any corrections to the vertical component in the time series due to these events.

[24] We fit the GIPSY/OASIS II and GAMIT/GLOBK time series with a comparable model as in equation (1). For the GIPSY/OASIS II time series we used the software tsview [*Herring*, 2003b], and for the GAMIT/GLOBK data we used a procedure described by *Nikolaidis* [2002]. Table 4 shows the ITRF2000 velocities of the permanent stations in Iceland from the GAMIT/GLOBK and GIPSY/OASIS II data processing and Table 5 lists the corresponding annual terms for the GIPSY/OASIS II time series. The ITRF2000 velocities from the GAMIT/GLOBK and GIPSY/OASIS II data processing agree well (within about 1 mm/yr) in the horizontal components (Table 4), except at station HLID where larger differences are caused by different approaches in estimating the coseismic offset at HLID (Figure 5). The agreement between the vertical velocities obtained by the different processing softwares is not as good as for the horizontal velocities.

[25] Velocity uncertainties are calculated in different ways for the time series obtained from the different processing softwares. For the GAMIT/GLOBK time series we assume white and flicker noise distribution [*Nikolaidis*, 2002; *Wdowinski et al.*, 2004], and for the GIPSY/OASIS II time series the velocity uncertainties are calculated using the sigmas of the coordinate estimates and the statistical properties of the time series residuals with white noise assumptions [*Herring*, 2003b] (Table 4). The velocity uncertainty for the Bernese data is based on the variance of the residuals, σ^2, after applying equation (1). The variance of the residuals is

$$\sigma^2 = \frac{\sum_{i=1}^{N} \{y_i - [a + bt + A\cos(\omega t + \phi)]\}^2}{(N-4)}, \quad (2)$$

where N is the number of data points. Here we estimate the velocity uncertainty, σ_{vel}, as

$$\sigma_{vel} = \sigma / T, \quad (3)$$

where T is the length of the time series in years. This approach can be compared to the approach of *Mao et al.* [1999]. Their equation (20) for the total rate uncertainty estimates from GPS data, assuming zero random walk error and long time spans, i.e., white noise error is insignificant, leads to $\sigma_{vel} \propto \sigma / T$. Following the approach and suggested

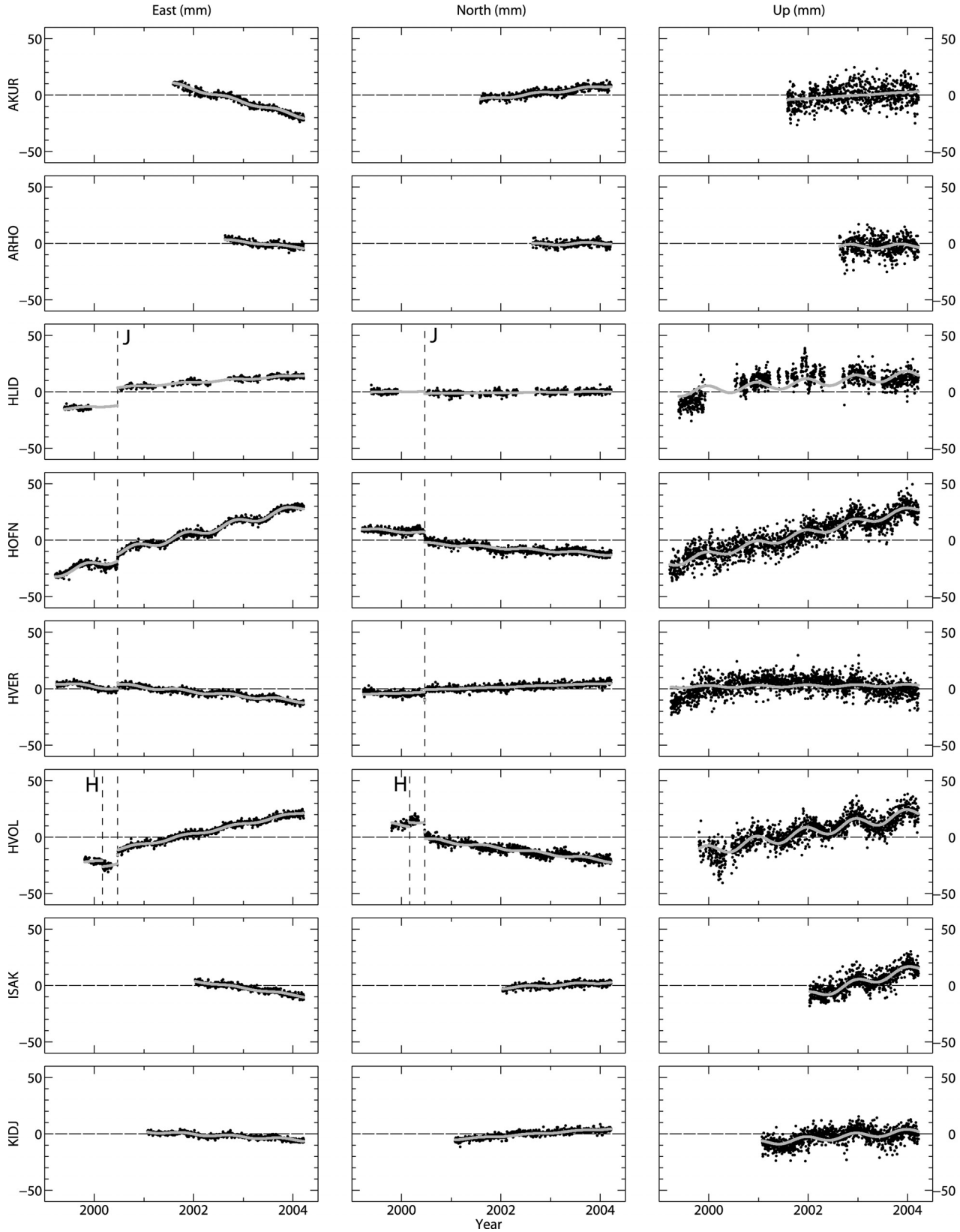

Figure 5. Time series for the CGPS stations in Iceland from the Bernese solutions, relative to REYK, showing east, north, and vertical solutions. The solid gray line shows the data fit from equation (1). The vertical dashed lines represent the times of the 17 and 21 June M_w = 6.5 earthquakes in 2000 (J), and the start of the Hekla eruption in February 2000 (H).

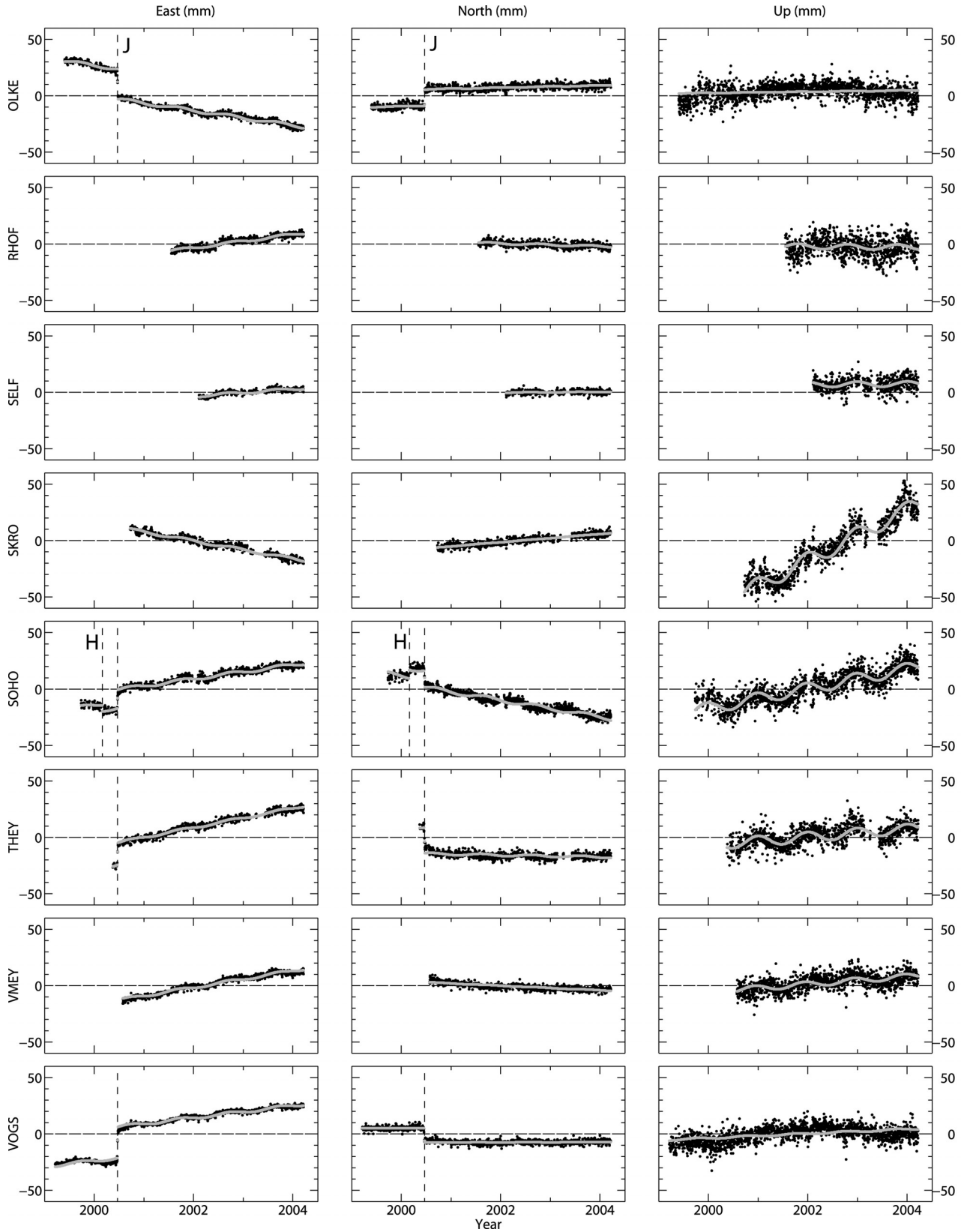

Figure 5. (continued)

noise level values of *Mao et al.* [1999], we would obtain uncertainties larger than resulting from equation (3) by a factor of 1.5 to 3. However, following the approach described by *Dixon et al.* [2000], obtaining the noise level values from a linear relation to the weighted RMS (Table 1), we would obtain uncertainties that are up to a factor of 1.9 smaller than obtained by equation (3). The methods of *Mao et al.* [1999] and *Dixon et al.* [2000] can however not

Table 1. Calculated Velocities, With 1σ Uncertainties, of the Stations in East, North, and Up, Relative to REYK, From the Bernese Time Series Fit From Equation (1)

						Velocities,[d] mm/yr			WRMS,[e] mm		
Station	Latitude	Longitude	H,[a] m	T,[b] years	Dn,[c] days	E	N	U	E	N	U
AKUR	65.69	−18.12	134	2.63	813	−0.6 ± 0.6	3.1 ± 0.7	2.8 ± 2.9	1.5	1.6	7.4
ARHO	66.19	−17.11	124	1.58	517	6.1 ± 0.9	−0.8 ± 1.1	0.3 ± 4.5	1.4	1.6	6.7
HLID	63.92	−21.39	111	4.83	1032	13.5 ± 0.3	−1.2 ± 0.3	3.1 ± 1.6	1.1	1.4	7.4
HOFN	64.27	−15.20	83	5.00	1636	21.4 ± 0.4	−4.4 ± 0.4	9.7 ± 1.4	1.7	1.9	6.4
HVER	64.02	−21.18	150	4.98	1706	6.6 ± 0.3	−0.1 ± 0.3	0.2 ± 1.4	1.3	1.5	6.8
HVOL	63.53	−18.85	265	4.42	1417	19.3 ± 0.3	−6.9 ± 0.6	7.9 ± 1.5	1.4	2.4	5.9
ISAK	64.12	−19.75	319	2.19	757	4.3 ± 0.6	0.7 ± 0.6	11.2 ± 2.5	1.2	1.3	5.1
KIDJ	64.00	−20.77	123	3.14	1124	8.2 ± 0.3	1.5 ± 0.5	3.3 ± 1.7	1.0	1.3	5.2
OLKE	64.06	−21.22	551	4.82	1609	3.9 ± 0.3	−0.7 ± 0.4	0.6 ± 1.4	1.3	1.9	6.3
RHOF	66.46	−15.95	77	2.66	890	16.4 ± 0.6	−2.9 ± 0.7	−0.3 ± 3.2	1.6	1.7	8.1
SELF	63.93	−21.03	82	2.11	661	13.8 ± 0.6	−1.3 ± 0.6	0.2 ± 2.2	1.1	1.2	4.4
SKRO	64.56	−18.38	982	3.49	1063	2.6 ± 0.5	2.0 ± 0.5	22.5 ± 2.0	1.7	1.7	6.8
SOHO	63.55	−19.25	857	4.48	1443	16.8 ± 0.4	−9.1 ± 0.7	8.7 ± 1.4	1.6	3.0	6.1
THEY	63.56	−19.64	195	3.84	1160	19.1 ± 0.4	−2.5 ± 0.6	3.5 ± 1.6	1.6	2.1	5.7
VMEY	63.43	−20.29	135	3.64	1292	18.0 ± 0.4	−3.7 ± 0.5	3.5 ± 1.5	1.5	1.6	5.2
VOGS	63.85	−21.70	73	5.00	1722	15.9 ± 0.3	−1.6 ± 0.3	2.0 ± 1.2	1.2	1.4	5.9

[a]Ellipsoidal height.
[b]Length of time series.
[c]Number of station days in time series.
[d]The parameter b in equation (1).
[e]Weighted RMS of residuals of data fit.

be applied directly to our data set because of different processing strategies. Equation (3) is our preferred velocity uncertainty estimate, giving a more realistic estimation of uncertainties than assuming simply white noise.

[26] In the time series shown in Figure 5, outliers have been removed and the fit from equation (1) is drawn in gray with the data. The time series span the period from the beginning of measurements to 18 March 2004. The longest time series spans exactly 5 years (VOGS), whereas other stations span shorter time intervals.

[27] A significant coseismic deformation signal, seen as offsets in the time series (Figure 5 and Table 3), was observed at all operational ISGPS stations due to the June 2000 earthquake sequence [*Árnadóttir et al.*, 2001, 2004, 2006]. Small coeruptive displacements are observed at SOHO and HVOL due to an eruption that started on 26 February 2000 in Hekla volcano, located approximately 45 km NW of the stations.

2.4. Seasonal Signals

[28] A pronounced feature in the east and vertical components of the time series (Figure 5), are seasonal signals. They have been identified in several studies of continuous GPS time series and are often suggested to be caused by various seasonal loading sources such as atmosphere, snow, groundwater, nontidal ocean loading, soil moisture, and temperature variations [e.g., *Heki*, 2001; *Dong et al.*, 2002; *Heki*, 2004; *Prawirodirdjo et al.*, 2006]. We model these signals as cosine functions of a fixed amplitude and phase in time (Table 2). The seasonal signal is generally smallest in the north component (Table 2) except at station SOHO. The movement of SOHO is possibly affected by magma accumulation at shallow depth in the Katla volcano and seasonal ice load changes of Mýrdalsjökull glacier (V. Pinel et al., Green's function estimates of Earth response to variable surface loads: Application to deformation of the subglacial Katla volcano, Iceland, submitted to *Geophysical Journal International*, 2006, hereinafter referred to as Pinel et al., submitted manuscript, 2006). The seasonal signal can be seen clearly in the east and vertical components at many stations in the Bernese processing (e.g., HOFN and HVOL, Figure 5). The stations are all moving in phase in the east component, but the amplitude differs somewhat between stations, ranging from 0.6 mm for ARHO to 3.0 mm for HOFN (Table 2). We also observe seasonal signals in the GIPSY/OASIS II time series (Table 5). In the east component our reference station for the Bernese processing, REYK, has the largest seasonal amplitude in the GIPSY/OASIS II processing (Table 5). Moreover, it is 180° out of phase with the station that shows the second largest annual amplitude (HOFN), so when using REYK as a reference

Table 2. Calculated Station Annual Terms From the Bernese Time Series, as in Equation (1)

	Amplitude,[a] mm			Phase,[b] rad		
Station	E	N	U	E	N	U
AKUR	1.23	1.04	0.13	4.37	4.53	1.42
ARHO	0.59	1.06	1.95	4.90	4.41	0.91
HLID	0.65	0.20	3.87	4.76	1.67	0.32
HOFN	3.00	0.87	3.16	5.23	2.83	5.70
HVER	1.18	0.18	0.97	4.36	2.48	6.11
HVOL	1.09	1.15	4.83	5.07	1.96	5.87
ISAK	0.66	0.85	3.66	4.74	3.28	5.98
KIDJ	0.99	0.49	2.43	4.71	2.85	0.36
OLKE	1.27	0.26	0.25	4.45	0.51	1.12
RHOF	1.10	0.79	2.32	4.86	4.83	1.23
SELF	1.10	0.23	2.35	4.27	3.49	0.01
SKRO	1.06	0.16	7.10	5.19	3.61	6.06
SOHO	1.39	1.56	5.20	4.68	1.86	6.01
THEY	0.96	0.89	4.38	4.58	2.43	0.06
VMEY	1.12	0.20	2.41	4.36	1.57	0.44
VOGS	1.25	0.10	0.70	4.56	3.34	1.51

[a]A in equation (1).
[b]The parameter ϕ in equation (1).

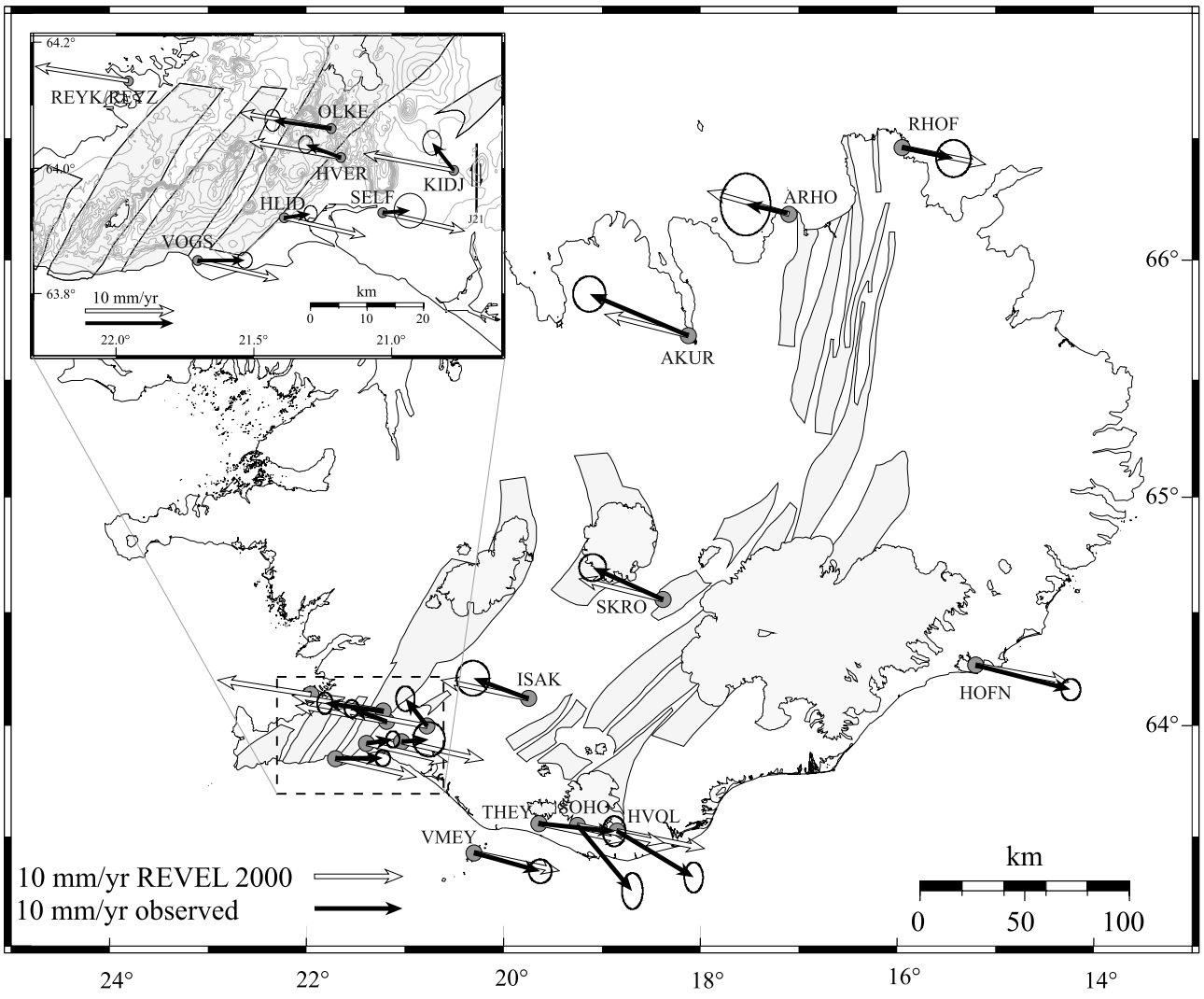

Figure 6. Horizontal velocities of CGPS stations in Iceland calculated from the time series shown in Figure 5. The velocities are translated into a local reference frame assuming that REYK moves at 10.5 mm/yr and 1.6 mm/yr in east and north, respectively (black arrows). The white arrows show the predicted REVEL plate motion. The ellipses represent the 2σ confidence level. The inset figure shows an enlarged map of the Hengill triple junction in SW Iceland. The N-S striking fault that ruptured in the 21 June 2000 main shock is shown (J21).

station the annual signals at HOFN and REYK add constructively. We suggest that a major part of the E-W seasonal signals observed in the Bernese time series (Figure 5) are caused by E-W seasonal motion of REYK.

[29] The vertical seasonal movements are all in phase (Tables 2 and 5), with a maximum in late November. When the seasonal amplitude is small, the phase cannot be estimated accurately. In the vertical component, the station REYK has a similar amplitude as the other stations (Table 5) and can thus not be the source of the vertical seasonal signal observed in the Bernese time series. We suggest that water and snow loading may contribute to the observed seasonal signals in Iceland, as suggested elsewhere by a number of authors. A separate study of the annual cycle of deformation at Katla volcano suggests that the annual load in the overlying Mýrdalsjökull ice cap may contribute significantly to the annual cycle of deformation at the SOHO continuous GPS station. The apparent annual cycle in widening across Iceland as suggested by the data from REYK and HOFN may eventually relate to snow load in the interior of Iceland. The order of magnitude of such a cycle can be estimated by assuming a disk load corresponding to about the size of the Icelandic highland (R_0 = 150 km), with h = 1 m of water equivalent snow load (in reality it is known to vary from a few centimeters to several meters). Subsidence under a disk load on the surface of an elastic half-space is maximum at its center, equal to:

$$U_{z,center} = 2\rho h R_0 g \frac{1-\nu^2}{E}, \tag{4}$$

where ν is the Poisson's ratio (set to 0.25) and E is the Young's modulus. This equation can, e.g., be derived from the convolution of a disk load with a Green's function for

Table 3. Calculated Offsets of the Stations in East, North, and Up, Relative to REYK From the Bernese Data Processing[a]

Station	Time	Event	E, mm	N, mm	U, mm
HVER	2000.4634	J17	6.3 ± 0.9	−5.2 ± 1.3	−0.0 ± 5.5
HOFN	2000.4634	J17	8.1 ± 1.5	−4.0 ± 1.4	−2.4 ± 5.8
HVOL	2000.4634	J17	8.9 ± 1.5	−7.8 ± 1.8	4.1 ± 7.3
OLKE	2000.4634	J17	−10.3 ± 1.1	2.6 ± 1.4	0.1 ± 5.9
SOHO	2000.4634	J17	9.4 ± 1.1	−8.1 ± 1.3	−3.4 ± 5.5
THEY	2000.4634	J17	12.3 ± 1.1	−12.4 ± 1.4	−1.6 ± 5.6
VOGS	2000.4634	J17	18.9 ± 0.9	−10.6 ± 1.2	0.4 ± 5.4
HVER	2000.4727	J21	−1.9 ± 0.9	9.0 ± 1.3	2.3 ± 5.5
HOFN	2000.4727	J21	3.5 ± 1.5	−3.4 ± 1.3	4.4 ± 5.5
HVOL	2000.4727	J21	3.9 ± 1.1	−3.4 ± 1.3	−0.0 ± 5.6
OLKE	2000.4727	J21	−13.6 ± 1.1	12.8 ± 1.4	−4.0 ± 5.8
SOHO	2000.4727	J21	5.1 ± 1.1	−6.0 ± 1.3	5.6 ± 5.5
THEY	2000.4727	J21	6.4 ± 1.1	−5.5 ± 1.4	−0.2 ± 5.8
VOGS	2000.4727	J21	8.8 ± 0.9	0.8 ± 1.3	5.5 ± 5.4
HLID	2000.4634	J17 and J21	15.7 ± 3.0	−1.9 ± 3.0	0 ± 6.0
HVOL	2000.1575	Hekla	−2.3 ± 0.9	1.8 ± 1.0	−4.1 ± 3.7
SOHO	2000.1575	Hekla	0.4 ± 0.9	4.5 ± 1.0	−5.9 ± 3.5

[a]Uncertainties are at the 1σ level. Events J17 and J21 are the 17 and 21 June 2000 main shocks and triggered earthquakes. Event Hekla is the Hekla eruption in February 2000.

Table 5. Calculated Annual Amplitudes and Phases of the GIPSY/OASIS II Time Series, in ITRF2000

	Amplitude, mm			Phase, rad		
Station	E	N	U	E	N	U
AKUR	0.88	1.07	3.98	3.11	4.54	5.64
ARHO	0.74	1.12	3.98	2.84	4.38	5.41
HLID	2.17	1.27	2.67	1.47	2.00	6.22
HOFN	1.47	0.89	6.45	5.59	2.18	5.88
HVER	0.18	0.21	3.92	0.86	5.22	5.74
HVOL	0.90	0.97	6.03	0.96	2.25	5.93
ISAK	0.90	0.98	5.39	1.34	3.42	5.71
KIDJ	0.50	0.29	3.70	1.07	3.04	5.67
OLKE	0.58	0.22	2.95	2.93	5.76	5.90
REYK	2.19	0.40	3.72	1.75	0.93	6.02
REYZ	3.29	0.51	3.28	1.10	0.73	0.21
RHOF	0.17	0.78	2.50	3.50	3.98	5.65
SELF	0.46	0.40	4.02	2.46	3.45	5.91
SKRO	1.44	1.10	8.07	0.89	3.94	5.86
SOHO	0.48	1.36	8.16	0.47	1.92	5.59
THEY	1.47	0.81	6.09	0.34	2.85	5.90
VMEY	0.68	0.22	3.27	1.54	3.42	5.74
VOGS	0.43	0.32	2.55	1.19	3.99	0.02

Table 4. Calculated Velocities of the Stations in East, North, and Up, Relative to the ITRF2000 Reference Frame, From the GAMIT/GLOBK and GIPSY/OASIS II Softwares[a]

	Velocities, mm/yr			
Station	E	N	U	So[b]
AKUR	−10.77 ± 0.20	22.51 ± 0.14	5.57 ± 0.36	GO
	−9.75 ± 0.14	23.39 ± 0.09	3.55 ± 1.27	GG
ARHO	−2.41 ± 0.28	19.44 ± 0.21	3.85 ± 0.62	GO
	−2.20 ± 0.63	19.93 ± 0.43	6.43 ± 5.30	GG
HLID	5.33 ± 0.22	21.32 ± 0.15	4.66 ± 0.41	GO
	2.35 ± 0.02	18.78 ± 0.02	−1.96 ± 0.26	GG
HOFN	11.79 ± 0.10	15.53 ± 0.08	8.95 ± 0.21	GO
	11.91 ± 0.02	15.50 ± 0.01	7.86 ± 0.13	GG
HVER	−4.63 ± 0.10	19.25 ± 0.07	−3.49 ± 0.19	GO
	−4.01 ± 0.02	19.45 ± 0.01	−6.16 ± 0.16	GG
HVOL	8.33 ± 0.09	12.23 ± 0.07	10.41 ± 0.21	GO
	8.09 ± 0.02	12.39 ± 0.02	4.01 ± 0.26	GG
ISAK	−6.02 ± 0.17	20.22 ± 0.14	11.72 ± 0.37	GO
	−5.66 ± 0.19	20.60 ± 0.13	14.23 ± 1.73	GG
KIDJ	−2.85 ± 0.09	20.36 ± 0.07	3.08 ± 0.18	GO
	−2.55 ± 0.05	20.70 ± 0.04	2.10 ± 0.50	GG
OLKE	−7.32 ± 0.09	18.44 ± 0.07	−2.33 ± 0.17	GO
	−7.39 ± 0.02	18.93 ± 0.01	−2.86 ± 0.16	GG
REYK	−12.59 ± 0.11	19.48 ± 0.09	−2.00 ± 0.25	GO
	−11.35 ± 0.01	19.78 ± 0.01	−5.80 ± 0.11	GG
REYZ	−11.67 ± 0.14	19.80 ± 0.07	−2.63 ± 0.18	GO
	−11.51 ± 0.09	20.31 ± 0.07	−4.06 ± 1.01	GG
RHOF	7.64 ± 0.13	15.72 ± 0.12	7.20 ± 0.37	GO
	7.80 ± 0.11	16.28 ± 0.08	1.22 ± 0.95	GG
SELF	2.66 ± 0.26	18.19 ± 0.20	3.06 ± 0.50	GO
	2.64 ± 0.26	18.11 ± 0.20	4.28 ± 2.54	GG
SKRO	−8.32 ± 0.09	21.40 ± 0.07	20.75 ± 0.19	GO
	−7.65 ± 0.05	21.94 ± 0.03	19.84 ± 0.41	GG
SOHO	5.47 ± 0.08	10.10 ± 0.07	11.63 ± 0.20	GO
	5.89 ± 0.02	10.75 ± 0.02	4.53 ± 0.22	GG
THEY	8.06 ± 0.08	16.54 ± 0.07	0.42 ± 0.17	GO
	8.54 ± 0.04	16.84 ± 0.03	5.12 ± 0.45	GG
VMEY	6.73 ± 0.08	15.56 ± 0.06	1.37 ± 0.17	GO
	7.07 ± 0.04	15.65 ± 0.03	0.92 ± 0.43	GG
VOGS	4.57 ± 0.08	17.88 ± 0.06	0.57 ± 0.19	GO
	5.58 ± 0.02	17.64 ± 0.01	−4.11 ± 0.18	GG

[a]Uncertainties are at the 1σ level.
[b]Software, GO is from GIPSY/OASIS II, and GG is from GAMIT/GLOBK.

response to a unit point mass applied on an elastic half-space (Pinel et al., submitted manuscript, 2006). The response scales inversely with the Young's modulus. For the above load and the static Young's modulus set equal to 60 GPa [*Sigmundsson et al.*, 2005], the maximum vertical displacement in the center of Iceland would be about 4.5 cm. The subsidence would decay away from the center of the island, but nowhere would the horizontal displacement exceed 1/3 of the value of the vertical (Pinel et al., submitted manuscript, 2006). For this load and Young's modulus, horizontal displacements would be less than 15 mm (peak to peak amplitude). A more detailed study of this effect is needed as the actual distribution of the snow load is poorly constrained. Such a study is outside the scope of this paper. Furthermore, although apparent east-west extension occurs across Iceland based on the REYK-HOFN line, then similar east-west change is observed between REYK and VOGS, with the VOGS station being close to REYK. Other sources of loading may contribute, including atmospheric and oceanic loading such as a major oscillation in atmospheric pressure centered just south of Iceland (the North Atlantic Oscillation).

3. Station Velocities and Plate Spreading

[30] The ISGPS station velocities provide a large-scale view of the plate movements in Iceland. Although the number of stations is small, compared to campaign GPS measurements, the distribution allows us to draw a number of conclusions from the data in this study. The plate movements, seen as gradual displacements toward east and south for stations on the Eurasian plate (HLID, VOGS, SELF, VMEY, THEY, SOHO, HVOL, HOFN, and RHOF) and toward west and north for stations on the North American plate (HVER, OLKE, ISAK, SKRO, and AKUR), dominate the velocities (Figure 6 and Table 1). The horizontal velocities are in general agreement with plate motion models such as the REVEL model [*Sella et al.*, 2002] and NUVEL-1A [*DeMets et al.*, 1994], but discrepancies are

observed at stations within the plate boundary deformation zone in north and south Iceland (Figure 6). The width of the plate boundary deformation zones in Iceland is on the order of 100 km wide, where a majority (~90%) of the plate spreading is achieved [e.g., *Heki et al.*, 1993; *LaFemina et al.*, 2005; *Geirsson et al.*, 2005].

[31] Oblique spreading across the eastern part of the Reykjanes Peninsula (RP) and the south Iceland seismic zone (SISZ) is well documented by CGPS data in SW Iceland. The stations in SW Iceland (Figure 6, inset) are within the plate boundary deformation zone, with lower station velocities close to the center of the zone. A change in direction between the velocities of HLID and HVER, SELF and KIDJ, and VMEY and ISAK suggests that the center of the plate boundary lies between these stations, with HLID, SELF, and VMEY to the south and HVER, KIDJ, and ISAK to the north. Stations OLKE and VOGS are further from the plate boundary, but still within the deformation zone as they are not moving at the full REVEL spreading rate. Our continuous GPS network is too sparse to estimate a kinematic model of plate spreading at the Hengill triple junction, as it is a complex area. A kinematic model has been constructed for this area, based on velocities from GPS campaign observations (1992 to 1999) [*Árnadóttir et al.*, 2006]. Assuming an elastic half-space dislocation model with E-W left-lateral motion along the RP and SISZ and opening across the WVZ, they find a locking depth of about 8 km below the Reykjanes Peninsula and 16 km below the SISZ, with deep slip rates ranging from 17 to 19 mm/yr, as well as a small component of opening (about 9 mm/yr) across the Reykjanes Peninsula. The other stations in south Iceland, VMEY, THEY, SOHO, and HVOL, are located on the Eurasian plate, but the velocities of SOHO and HVOL are disturbed by local sources (see section 5).

[32] The only station in SW Iceland showing significant deviation from the azimuth predicted by the REVEL model is KIDJ, located approximately 5 km west of the fault that ruptured on 21 June 2000 (Figure 6, inset). The motion of KIDJ is affected by postseismic deformation due to the June 2000 earthquakes [*Árnadóttir et al.*, 2005]. The northward velocity of KIDJ has decreased from 4.7 ± 1.8 mm/yr during 2001 to 2002.5, to 2.1 ± 1.8 mm/yr during 2002.5 to 2004.18. The deformation signal captured by campaign and continuous GPS observations in the SISZ from 2000 to 2004, can be explained by either afterslip below the 17 and 21 June coseismic ruptures or viscoelastic relaxation in the lower crust and upper mantle [*Árnadóttir et al.*, 2005].

[33] Partitioning of spreading between the eastern and western volcanic zones (Figure 1) has implications for strain accumulation and seismic hazard in the SISZ. We do not have any profiles crossing the WVZ, but the EVZ is located between stations ISAK and HVOL in the southern part, and SKRO and HOFN in the northern part. The spreading between ISAK and HVOL is 15.1 ± 1.7 mm/yr and between SKRO and HOFN the spreading is 18.8 ± 1.2 mm/yr, indicating that at the latitude of SKRO the EVZ is accommodating the full spreading across Iceland. This is in general agreement with *LaFemina et al.* [2005], who observe spreading rates across the EVZ of 11.0 ± 0.8 mm/yr in the southern part and 19.9 ± 2.0 mm/yr in its northern part from GPS campaign measurements. EDM and GPS campaign measurements made in 1967 to 1994 along a profile across the southern part of the EVZ show extension of about 12 mm/yr [*Jónsson et al.*, 1997]. Magma accumulation in Hekla and Katla would act to increase the observed spreading rates between ISAK and HVOL, so our estimate is an upper bound on the current spreading rate across the southern part of the EVZ.

[34] The CGPS network in northern Iceland can give constraints on strain partitioning between active fault zones, where the tectonic setting is more complicated than in south Iceland (Figure 1). Results from GPS campaigns made in northern Iceland indicate that the velocity field may change substantially with time (F. Jouanne et al., Rift-transform junction in north-Iceland: Rigid blocks and narrow accommodation zones revealed by GPS 1997–1999–2002, submitted to *Geophysical Journal International*, 2006). Station AKUR is moving with the North American plate and RHOF with the Eurasian plate (Figure 6). The observed velocity between AKUR and RHOF is 18.1 ± 1.2 mm/yr in direction N109.3°E ± 4.2° relative to AKUR, or 93 ± 6% of the total spreading between the two stations predicted by the REVEL model. Station ARHO is located between the two main strands of the Tjörnes fracture zone (TFZ), the Húsavík-Flatey fault (HFF) and the Grímsey lineament (GL, Figure 1) and is moving at an intermediate velocity. The observed velocity between AKUR and ARHO is 7.8 ± 1.5 mm/yr in direction N119.3°E ± 7.8° relative to AKUR, indicating that a similar amount of strain is being accumulated at the HFF and the GL.

4. Vertical Movements

[35] The CGPS observations reveal significant vertical rates of uplift, relative to REYK (Figure 7 and Table 1). Similar results are derived from the GIPSY/OASIS II and GAMIT/GLOBK solutions, where the rates are estimated in the ITRF2000 (Table 4). *Sella et al.* [2002] report vertical velocities of −3.4 ± 1.5 mm/yr for REYK and 4.0 ± 2.3 mm/yr for HOFN. A tide gauge record in Reykjavík shows a sea level rise of 2.4 to 3.4 mm/yr [*Einarsson*, 1994], at about the same rate as the inferred geocentric subsidence rate at the REYK continuous station. Accordingly, most of the relative sea level rise in Reykjavík may be caused by land subsidence. The lack of eustatic component to sea level change in Reykjavík may reflect the relatively large variability in sea level rise around the globe as witnessed, e.g., by satellite altimetery measurements and interpretations of *Cazenave and Nerem* [2004].

[36] The vertical velocities indicate a maximum uplift rate near the center of Iceland, with the station SKRO moving up at a rate of more than 20 mm/yr, relative to REYK. A similar rate of uplift is observed for GPS campaigns in Central Iceland [*LaFemina et al.*, 2005; *Geirsson et al.*, 2005], confirming that the high vertical rate of SKRO is not caused by monument instability. Uplift rates of 6 mm/yr have been observed in the Svalbard Islands [*Hagedoorn and Wolf*, 2003] and up 30 mm/yr to in Glacier Bay, Alaska [*Larsen et al.*, 2005]. These studies suggest that the rapid uplift rates are caused by recent retreat of glaciers due to global warming. The vertical rates of SKRO, HOFN, and ISAK are comparable with results from studies of ongoing crustal rebound which suggest a present crustal uplift rate of 5–15 mm/yr in the area around Vatnajökull ice cap due to

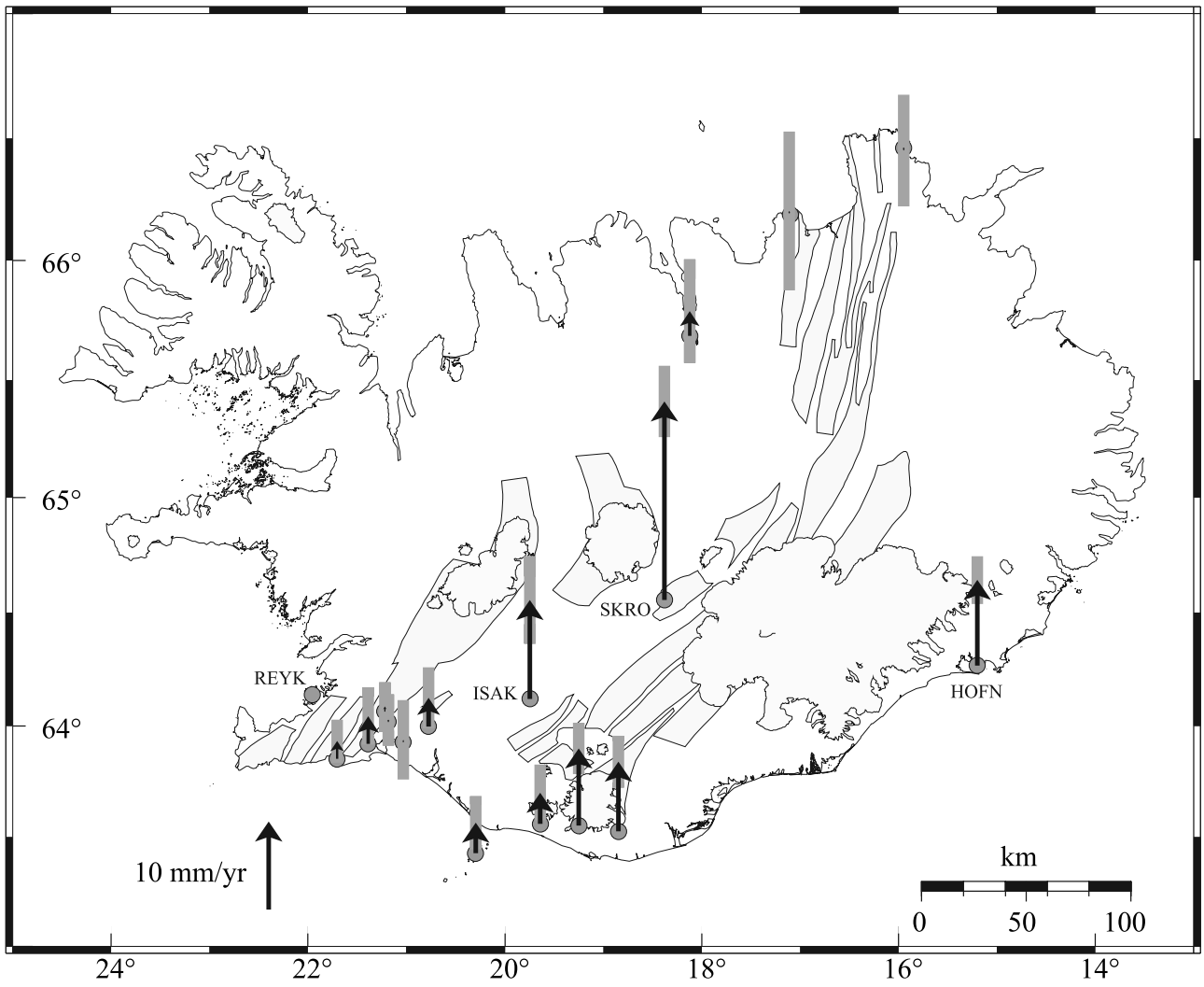

Figure 7. Vertical velocities of the CGPS stations, assuming REYK is fixed (Table 1). Confidence limits are at the 2σ level, shown with gray bars around the arrow heads. All the stations with significant velocities are moving up relative to REYK, with increasing velocities toward the center of the island.

retreat and thinning of the ice cap [*Sigmundsson and Einarsson*, 1992; *Sjöberg et al.*, 2004; C. Pagli et al., Glacio-isostatic deformation around the Vatnajökull ice cap, Iceland, induced by recent climate warming: GPS observations and finite element modeling, submitted to *Journal of Geophysical Research*, 2006].

5. Discussion

[37] The plate spreading of the Mid-Atlantic Ridge across Iceland that we observe with CGPS is in good agreement with existing plate motion models based on geologic and geodetic data [*DeMets et al.*, 1994; *Sella et al.*, 2002]. This implies that the spreading rate outside the plate boundary deformation zone is stable on long and short timescales [*Sella et al.*, 2002] although major rifting episodes like the Krafla rifting event (1975–1984) in the NVZ may enhance the spreading rate temporarily at distances up to 50 to 75 km from the plate boundary [*Hofton and Foulger*, 1996].

[38] The June 2000 earthquake sequence in south Iceland (Figure 1), including two M_w = 6.5 earthquakes occurring on 17 and 21 June, caused a significant offset in the time series (Figure 5). *Árnadóttir et al.* [2001] estimated coseismic station displacements in the epicentral area from continuous and GPS campaign data from 1995, 1999, and 2000 (19–30 June). The coseismic displacements were then inverted to obtain the optimal fault geometries and slip on the 17 and 21 June ruptures. The observed offsets at stations to the east (THEY, SOHO, and HVOL) due to the 17 June earthquake (Table 3) agree fairly well with their model predictions. The fit is poor for stations OLKE, HVER, and VOGS due to local deformation caused by triggered events. Results from radar interferometry (InSAR) and GPS campaign measurements show deformation associated with three $M_W \geq 5$ earthquakes on Reykjanes Peninsula triggered by the 17 June main shock [*Pagli et al.*, 2003; *Árnadóttir et al.*, 2004]. The largest signal is observed near Lake Kleifarvatn (labeled Kl in Figure 1), suggesting that this event had the largest geodetic moment of the three Reykjanes events. The observed coseismic deformation at VOGS is therefore mostly due to the Kleifarvatn event [*Árnadóttir et al.*, 2004]. Furthermore, the geodetic studies

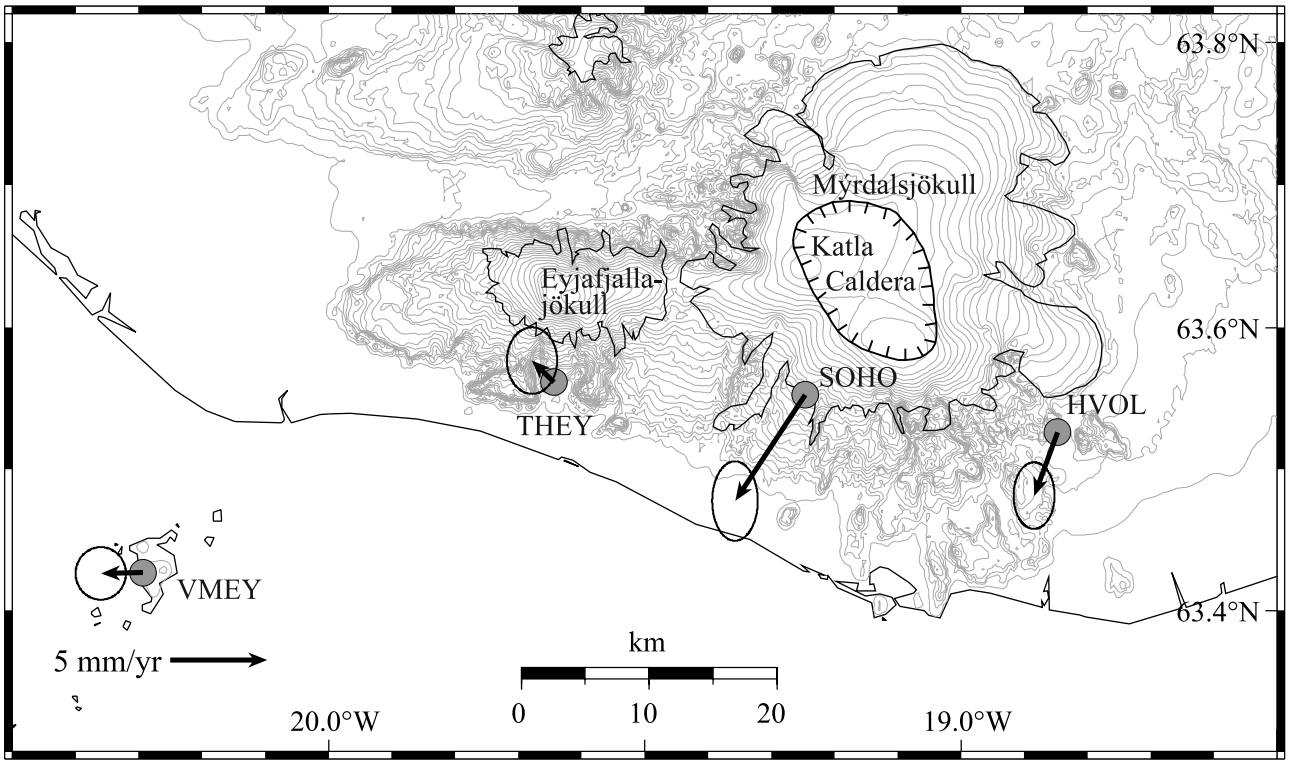

Figure 8. Residual horizontal velocities of stations in south Iceland, obtained by subtracting the motion of the Eurasian plate relative to the North American plate (from the REVEL model) from the observed velocities. The stations SOHO and HVOL show significant residual velocities outward from the Katla caldera.

conclude that the Kleifarvatn event had a significant component of aseismic slip [*Pagli et al.*, 2003; *Árnadóttir et al.*, 2004]. A seismic swarm was observed between stations OLKE and HVER in 17 June, and that may have caused some localized deformation.

[39] We have not found evidence for short-term preseismic displacements preceding the June 2000 earthquake sequence from the routine 24-hour data processing. We also searched for short-term preseismic signals by processing 4 weeks of data covering the earthquakes in 1-, 2-, and 3-hour batches using the Bernese software. The results show no indications of short-term preseismic signals.

[40] In south Iceland, the velocities of VMEY and THEY agree with the REVEL model prediction, but stations HVOL and in particular SOHO have a larger southward component than expected (Figures 8 and 9). Station SOHO is located approximately 10 km SW from the center of the caldera of Katla volcano, making it sensitive to pressure changes in a shallow magma reservoir under the caldera. Comparing north component of the time series from stations in south Iceland (SOHO, HVOL, THEY, and VMEY) reveals a more detailed picture of the movements. From Figure 9 we see that the stations closest to Katla (SOHO and HVOL) move episodically southward by about 5, 9, and 10 mm in the years 2001, 2002, and 2003, respectively. The duration of the southward movement varies from 2 months in 2001 to 8 months in 2003. GPS campaign measurements made on nunataks on the caldera rim suggest that the movements of SOHO and HVOL are caused by increasing pressure in a magma source, at a depth of 4–5 km, within the caldera [*Sturkell et al.*, 2003a, 2003b], although a significant fraction of the vertical displacements can be attributed to response to a recent reduction in ice load (Pinel et al., submitted manuscript, 2006).

[41] Small offsets are observed at SOHO and HVOL at the onset of the February 2000 Hekla eruption, located approximately 45 km NW of the stations. We estimate coeruptive offsets of 0.4 ± 0.6 mm in east and 4.5 ± 0.8 mm in north at SOHO and -2.3 ± 0.6 mm in east and 1.8 ± 0.8 mm in north at HVOL (Table 3). The offsets are directed toward Hekla, suggesting that the signals are caused by a pressure decrease in a deep magma chamber at the start of the eruption. We compared the displacements with independent modeling of the volcano source based on borehole strainmeters [*Ágústsson et al.*, 2000], which predicts coeruptive displacements of -1.2 mm in east and 3.2 mm in north for SOHO and -1.4 mm in east and 1.9 mm in north for HVOL, in broad agreement with our results.

[42] We find good agreement between data processing using three different high-level geodetic processing softwares. The Bernese solution is less dependent on reference frames and their stability than the other solutions. The weakest part of the Bernese processing strategy is the use of a single reference station. This means that data cannot be processed when the reference station is not operating and possible nontectonic movements of the reference station will corrupt the time series at all stations. Careful examination of the time series can be used to find common

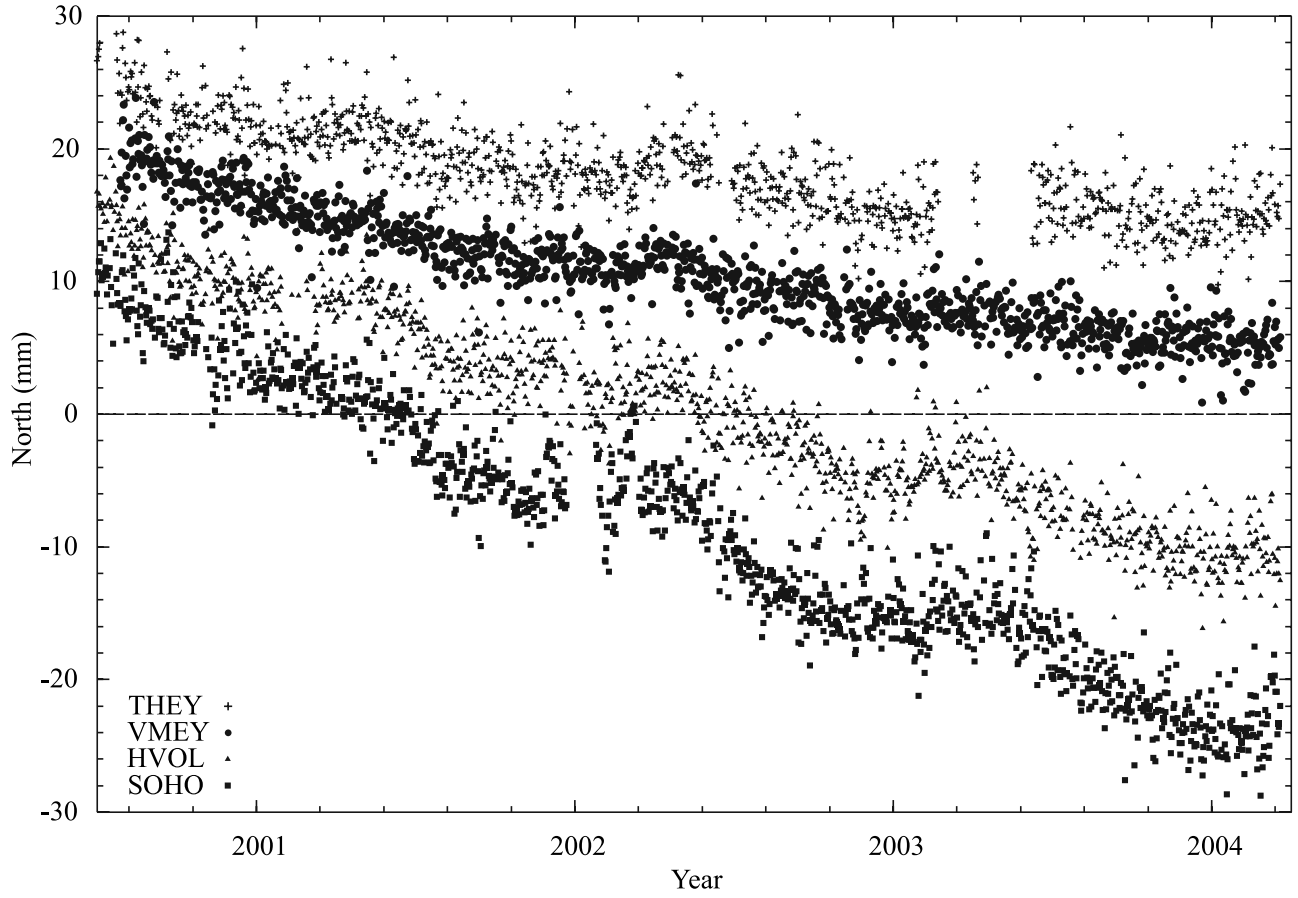

Figure 9. North component of the time series for stations THEY, VMEY, HVOL and SOHO in south Iceland, relative to REYK. The stations HVOL and in particular SOHO are moving episodically toward south. The boxes outline periods of accelerated southward motion at SOHO.

movements at all stations and this can be corrected for. We found three of these instances, all in the vertical component, due to equipment changes at REYK. We also use results from the GAMIT/GLOBK and GIPSY/OASIS II to verify that REYK is indeed a stable reference station on the long term. Its velocity has been found to be in agreement with the REVEL plate motion model [*Sella et al.*, 2002] and our results from the GAMIT/GLOBK and GIPSY/OASIS II processing support that. Hence our velocity estimates from data using REYK as the reference station are robust.

6. Conclusions

[43] We draw the following conclusions from our analysis of continuous GPS data from 18 stations in Iceland, spanning between 1.5 and 5 years:

[44] 1. Stations outside the ~100 km wide deformation zone surrounding the plate boundary show horizontal velocities that are consistent with plate motion models such as REVEL [*Sella et al.*, 2002] and NUVEL-1A [*DeMets et al.*, 1994]. Since the NUVEL-1A model is based on geological data spanning the last few million years, it appears that plate movements outside the deformation zones are steady on timescales ranging from weeks to millions of years.

[45] 2. An annual signal is superimposed on the long-term velocity trend. The annual signal is evident in the east and vertical components, with an amplitude as large as 10 mm. The annual signal in the east component is mostly due to the annual movement of the reference station, REYK. The origin of the vertical annual signal remains unexplained, although various loading effects have been suggested.

[46] 3. Stations within the plate boundary deformation zone are affected by various plate boundary processes, such as elastic stretching and strain accumulation due to the plate movements, coseismic deformation during earthquakes, volcanic deformation, postseismic and postrifting deformation. Signals due to these localized processes are superimposed on the overall plate velocities.

[47] 4. We have confirmed that the spreading in south Iceland occurs primarily across the Eastern volcanic zone. The crustal block between the Western and the Eastern Rifts, the Hreppar microplate, appears to be moving with the North American plate at present.

[48] 5. In north Iceland, the short time series of AKUR, ARHO, and RHOF indicate that more than half (60%) of the plate spreading is accommodated by the Grímsey lineament within the Tjörnes fracture zone, the remainder is mainly accommodated by strain accumulation across the Húsavík-Flatey fault.

[49] 6. Coseismic displacements were observed in the ISGPS network in association with the June 2000 south Iceland earthquake sequence, both due to the 17 and 21 June

main shocks, and earthquakes triggered on the Reykjanes Peninsula by the first event.

[50] 7. Small offsets were observed in the time series at the time of the February 2000 eruption in Hekla. The signals were seen at stations at 45 km distance, and are consistent with a rapid pressure decrease in a deep (~11 km) magma chamber below the volcano.

[51] 8. Observed station velocities on the south flank of Katla volcano deviate from the plate velocities, due to inflation of the volcano and changes in glacial load. These signals demonstrate the value of the continuous GPS stations for monitoring subglacial volcanoes.

[52] 9. Vertical rates show a clear trend. Most of the measured absolute rates are consistent with a slow subsidence (about 3 mm/yr) of the reference station in Reykjavík and a rapid uplift inland and near the ice caps in south Iceland. The station Skrokkalda (SKRO) has the largest uplift rate of about 20 mm/yr.

[53] **Acknowledgments.** We express our gratitude to all those who have participated in building up the ISGPS network. In particular, we thank Halldór Ólafsson for designing the ISGPS monument and taking part in installing most of the stations. We thank our technicians, in particular, Bergur H. Bergsson and Jósef Hólmjárn for their work. We thank all those numerous people who have given good advice on network operations and data processing. Installation cost for stations ARHO, RHOF, and SKRO was mainly supported by the European Commission (contract EVR1-CT1999-40002) and IFRTP (now IPEV, Arctic Program 316). We thank Kurt Feigl for fruitful discussion and his enthusiasm for using GAMIT/GLOBK to process the data. We are grateful to Tim Dixon and his colleagues at the University of Miami for their support and discussions. Comments from Sigrún Hreinsdóttir, Kosuke Heki, and an anonymous reviewer helped us improve the manuscript. The public domain GMT software [*Wessel and Smith*, 1991] was used to make the figures. This work was supported by EC funding from the RETINA (contract EVG1-CT-2001-0046), the PREPARED (EVG1-CT-2002-00073) and the FORESIGHT (GOCE-CT-2003-511139) projects.

References

Ágústsson, K., R. Stefánsson, A. T. Linde, P. Einarsson, I. S. Sacks, G. B. Gudmundsson, and B. Thorbjarnardóttir (2000), Successful prediction and warning of the 2000 eruption of Hekla based on seismicity and strain changes, *Eos Trans. AGU*, *81*(48), Fall Meet. Suppl., Abstract V11B-30.

Altamimi, Z., P. Sillard, and C. Boucher (2002), ITRF2000: A new release of the International Terrestrial Reference Frame for earth science applications, *J. Geophys. Res.*, *107*(B10), 2214, doi:10.1029/2001JB000561.

Árnadóttir, T., H. Geirsson, B. H. Bergsson, and C. Völksen (2000), The Icelandic continuous GPS network – ISGPS March 18, 1999 – February 20, 2000, report, Rit Vedurstofu Íslands, VÍ-R00002-JA02, Icelandic Meteorol. Off., Reykjavík.

Árnadóttir, T., S. Hreinsdóttir, G. B. Gudmundsson, P. Einarsson, M. Heinert, and C. Völksen (2001), Crustal deformation measured by GPS in the South Iceland Seismic Zone due to two large earthquakes in June 2000, *Geophys. Res. Lett.*, *28*(21), 4031–4033, doi:10.1029/2001GL013207.

Árnadóttir, T., H. Geirsson, and P. Einarsson (2004), Coseismic stress changes and crustal deformation on the Reykjanes Peninsula due to triggered earthquakes on June 17, 2000, *J. Geophys. Res.*, *109*, B09307, doi:10.1029/2004JB003130.

Árnadóttir, T., S. Jónsson, F. F. Pollitz, W. Jiang, and K. L. Feigl (2005), Postseismic deformation following the June 2000 earthquake sequence in the south Iceland seismic zone, *J. Geophys. Res.*, *110*, B12308, doi:10.1029/2005JB003701.

Árnadóttir, T., W. Jiang, K. L. Feigl, H. Geirsson, and E. Sturkell (2006), Kinematic models of plate boundary deformation in southwest Iceland derived from GPS observations, *J. Geophys. Res.*, *111*, B07402, doi:10.1029/2005JB003907.

Boucher, C., Z. Altamimi, and P. Sillard (1999), The 1997 International Terrestrial Reference Frame (ITRF97), *Tech. Note 27*, Int. Earth Rotation and Ref. Syst. Serv., Frankfurt, Germany.

Cazenave, A., and R. S. Nerem (2004), Present-day sea level change: Observations and causes, *Rev. Geophys.*, *42*, RG3001, doi:10.1029/2003RG000139.

Clifton, A. E., and P. Einarsson (2005), Styles of surface rupture accompanying the June 17 and 21, 2000 earthquakes in the South Iceland Seismic Zone, *Tectonophysics*, *369*, 141–159.

Clifton, A. E., C. Pagli, J. F. Jónsdóttir, K. Eythórsdóttir, and K. Vogfjörd (2003), Surface effects of triggered fault slip on Reykjanes Peninsula, SW Iceland, *Tectonophysics*, *369*, 145–154.

DeMets, C., R. G. Gordon, D. F. Argus, and S. Stein (1994), Effect of recent revisions to the geomagnetic reversal time scale on estimates of current plate motions, *Geophys. Res. Lett.*, *21*, 2191–2194.

Dixon, T. H., M. Miller, F. Farina, H. Wang, and D. Johnson (2000), Present-day motion of the Sierra Nevada block and some tectonic implications for the Basin and Range province, North American Cordillera, *Tectonophysics*, *19*, 1–24.

Dong, D., P. Fang, Y. Bock, M. K. Cheng, and S. Miyazaki (2002), Anatomy of apparent seasonal variations from GPS-derived site position time series, *J. Geophys. Res.*, *107*(B4), 2075, doi:10.1029/2001JB000573.

Einarsson, P. (1987), Compilation of earthquake fault plane solutions in the North Atlantic, in *Recent Plate Movements and Deformation*, *Geodyn. Ser.*, vol. 20, edited by K. Kasahara, pp. 47–62, AGU, Washington, D. C.

Einarsson, P. (1994), Crustal movements and relative sea level changes in Iceland, in *Proceedings of the Hornafjördur International Coastal Symposium*, edited by G. Viggósson, pp. 23–34, Icelandic Harbour Auth., Reykjavík.

Einarsson, P., and J. Eiríksson (1982), Earthquake fractures in the districts Land and Rangárvellir in the South Iceland Seismic Zone, *Joekull*, *32*, 113–119.

Einarsson, P., and K. Saemundsson (1987), Earthquake epicenters 1982–1985 and volcanic systems in Iceland, in *Í hlutarins edli*, edited by T. I. Sigfússon, map, Menningarsjódur, Reykjavík, Iceland.

Einarsson, P., S. Björnsson, G. R. Foulger, R. Stefánsson, and T. Skaftadóttir (1981), Seismicity pattern in the South Iceland seismic zone, in *Earthquake Prediction – An International Review*, *Maurice Ewing Series*, vol. 4, edited by D. Simpson and P. G. Richards, pp. 141–151, AGU, Washington, D. C.

Feigl, K. L., J. Gasperi, F. Sigmundsson, and A. Rigo (2000), Crustal deformation near Hengill volcano, Iceland, 1993–1998: Coupling between magmatic activity and faulting inferred from elastic modeling of satellite radar interferograms, *J. Geophys. Res.*, *105*, 25,655–25,670.

Foulger, G. R., R. Bilham, W. J. Morgan, and P. Einarsson (1986), The Iceland GPS geodetic field campaign 1986, *Eos Trans. AGU*, *68*, 1236.

Geirsson, H. (2003), Continuous GPS measurements in Iceland 1999–2002, *Rep. 03014*, 94 pp., Icelandic Meteorol. Off., Reykjavík.

Geirsson, H., et al. (2005), Crustal deformation in Iceland derived from the nation-wide 1993 and 2004 ISNET Campaigns, *Eos Trans. AGU*, *86*(52), Fall Meet. Suppl., Abstract G21B-1275.

Hagedoorn, J. M., and D. Wolf (2003), Pleistocene and recent deglaciation in Svalbard: Implications for tide-gauge, GPS and VLBI measurements, *J. Geodyn.*, *35*(4–5), 415–423, doi:10.1016/S02643707(03)000048.

Heki, K. (2001), Seasonal modulation of interseismic strain buildup in northeastern Japan driven by snow loads, *Science*, *293*, 89–92.

Heki, K. (2004), Dense GPS array as a new sensor of seasonal changes of surface loads, in *The State of the Planet: Frontiers and Challenges in Geophysics*, *Geophys. Monogr. Ser.*, vol. 150, edited by R. S. J. Sparks and C. J. Hawkesworth, pp. 177–196, AGU, Washington, D. C.

Heki, K., G. R. Foulger, B. R. Julian, and C. H. Jahn (1993), Plate dynamics near divergent boundaries: Geophysical implications of post-rifting crustal deformation in NE Iceland, *J. Geophys. Res.*, *98*(B8), 14,279–14,297.

Herring, T. (2003a), GLOBK: Global Kalman Filter VLBI and GPS analysis program version 4.1, report, Mass. Inst. of Technol., Cambridge.

Herring, T. (2003b), MATLAB Tools for viewing GPS velocities and time series, *GPS Solutions*, *7*(3), 194–199, doi:10.1007/s10291-003-0068-0.

Hofton, M. A., and G. R. Foulger (1996), Post-rifting anelastic deformation around the spreading plate boundary, north Iceland, 1: Modeling of the 1987–1992 deformation field using a viscoelastic Earth structure, *J. Geophys. Res.*, *101*, 25,403–25,421.

Hreinsdóttir, S., P. Einarsson, and F. Sigmundsson (2001), Crustal deformation at the oblique spreading Reykjanes peninsula, SW Iceland: GPS measurements from 1993 to 1998, *J. Geophys. Res.*, *106*, 13,803–13,816.

Hugentobler, U., S. Schaer, and P. Fridez (2001), Bernese GPS software version 4.2, Astron. Inst., Univ. of Bern, Bern, Switzerland.

Jónsson, S., P. Einarsson, and F. Sigmundsson (1997), Extension across a divergent plate boundary, the Eastern Volcanic Rift Zone, south Iceland, 1967–1994, observed with GPS and electronic distance measurements, *J. Geophys. Res.*, *102*, 11,913–11,929.

King, R. W., and Y. Bock (2003), Documentation for the GAMIT Analysis Software Release 10.6, report, Mass. Inst. of Technol., Cambridge.

LaFemina, P. C., T. H. Dixon, R. Malservisi, T. Árnadóttir, E. Sturkell, F. Sigmundsson, and P. Einarsson (2005), Geodetic GPS measurements in

south Iceland: Strain accumulation and partitioning in a propagating ridge system, *J. Geophys. Res.*, *110*, B11405, doi:10.1029/2005JB003675.

Larsen, C. F., R. J. Motyka, J. T. Freymueller, K. A. Echelmeyer, and E. R. Ivins (2005), Rapid viscoelastic uplift in southeast Alaska caused by post-Little Ice Age glacial retreat, *Earth Planet. Sci. Lett.*, *237*, 548–560.

Mao, A., C. G. A. Harrison, and T. H. Dixon (1999), Noise in GPS coordinate time series, *J. Geophys. Res.*, *104*, 2797–2816.

McClusky, S., et al. (2000), Global Positioning System constraints on plate kinematics and dynamics in the eastern Mediterranean and Caucasus, *J. Geophys. Res.*, *105*, 5695–5720.

Mervart, L. (1995), Ambiguity resolution technique in geodetic and geodynamic applications of the Global Positioning System, *Rep. 53*, Geodätisch-geophysikalische Arbeiten in der Schweiz, Zurich, Switzerland.

Nikolaidis, R. (2002), Observation of geodetic and seismic deformation with the Global Positioning System, Ph.D. thesis, Scripps Inst. of Oceanogr., La Jolla, Calif.

Pagli, C., R. Pedersen, F. Sigmundsson, and K. L. Feigl (2003), Triggered fault slip on June 17, 2000 on the Reykjanes Peninsula, SW-Iceland captured by radar interferometry, *Geophys. Res. Lett.*, *30*(6), 1273, doi:10.1029/2002GL015310.

Pedersen, R., F. Sigmundsson, K. L. Feigl, and T. Árnadóttir (2001), Coseismic interferograms of two Ms = 6. 6 earthquakes in the South Iceland Seismic Zone, June 2000, *Geophys. Res. Lett.*, *28*, 3341–3344.

Prawirodirdjo, L., Y. Ben-Zion, and Y. Bock (2006), Observation and modeling of thermoelastic strain in Southern California Integrated GPS Network daily position time series, *J. Geophys. Res.*, *111*, B02408, doi:10.1029/2005JB003716.

Rögnvaldsson, S. T., Á. Gudmundsson, and R. Slunga (1998), Seismotectonic analysis of the Tjörnes Fracture Zone, an active transform fault in north Iceland, *J. Geophys. Res.*, *103*, 30,117–30,129.

Schmidt, M., H. Dragert, Y. Lu, and B. Schofield (2003), The effect of SCIGN domes on the vertical antenna phase centre position, *Eos Trans. AGU*, *84*(46), Fall Meet. Suppl., Abstract G52B-0042.

Sella, G. F., T. H. Dixon, and A. Mao (2002), REVEL: A model for Recent plate velocities from space geodesy, *J. Geophys. Res.*, *107*(B4), 2081, doi:10.1029/2000JB000033.

Sigmundsson, F., and P. Einarsson (1992), Glacio-isostatic crustal movements caused by historical volume change of the Vatnajokull ice cap, Iceland, *Geophys. Res. Lett.*, *19*, 2123–2126.

Sigmundsson, F., P. Einarsson, R. Bilham, and E. Sturkell (1995), Rift-transform kinematics in south Iceland: Deformation from Global Positioning System measurements, 1986 to 1992, *J. Geophys. Res.*, *100*, 6235–6248.

Sigmundsson, F., P. Einarsson, S. T. Rögnvaldsson, G. Foulger, K. Hodkinson, and G. Thorbergsson (1997), The 1994–1995 seismicity and deformation at the Hengill triple junction, Iceland: Triggering of earthquakes by an inflating magma chamber in a zone of horizontal shear stress, *J. Geophys. Res.*, *102*, 15,151–15,161.

Sigmundsson, F., R. Pedersen, K. L. Feigl, V. Pinel, and H. Björnsson (2005), Glacial surges flex the crust of the Earth: Crustal deformation associated with rapid ice flow and mass redistribution at Icelandic outlet glaciers observed by InSAR, *Eos Trans. AGU*, *86*(52), Fall Meet. Suppl., Abstract G42A-07.

Sigurdsson, O., S. Zóphóníasson, and E. Ísleifsson (2000), A glacial flood from Sólheimajökull on 18 July 1999 (in Icelandic), *Joekull*, *49*, 75–80.

Sjöberg, L. E., M. Pan, S. Erlingsson, E. Asenjo, and K. Árnason (2004), Land uplift near Vatnajökull, Iceland, as observed by GPS in 1992, 1996 and 1999, *Geophys. J. Int.*, *159*, 943–948, doi:10.1111/j.1365I-246X.2004.02353.x.

Stefánsson, R., G. B. Gudmundsson, and P. Halldórsson (2003), The South Iceland earthquakes 2000 – A challenge for earthquake prediction research, *Rep. VI-R03017*, Icelandic Meteorol. Off., Reykjavík.

Sturkell, E., F. Sigmundsson, and P. Einarsson (2003a), Recent unrest and magma movements at Eyjafjallajökull and Katla volcanoes, Iceland, *J. Geophys. Res.*, *108*(B8), 2369, doi:10.1029/2001JB000917.

Sturkell, E., F. Sigmundsson, P. Einarsson, H. Geirsson, and M. J. Roberts (2003b), Magma inflow into Katla, one of Iceland's most hazardous volcanoes, *Eos Trans. AGU*, *84*(46), Fall Meet. Suppl., Abstract V12G-07.

Wdowinski, S., Y. Bock, G. Baer, L. Prawirodirdjo, N. Bechor, S. Naaman, R. Knafo, Y. Forrai, and Y. Melzer (2004), GPS measurements of current crustal movements along the Dead Sea Fault, *J. Geophys. Res.*, *109*, B05403, doi:10.1029/2003JB002640.

Webb, F. H., and J. F. Zumberge (1993), An introduction to GIPSY/OASIS-II precision software for the analysis of data from the Global Positioning System, *JPL Publ., D-11088*.

Wessel, P., and W. H. F. Smith (1991), Free software helps map and display data, *Eos Trans. AGU*, *72*, 441, 445–446.

Zumberge, J. F., M. B. Heflin, D. C. Jefferson, M. M. Watkins, and F. Webb (1997), Precise point positioning for the efficient and robust analysis of GPS data from large networks, *J. Geophys. Res.*, *102*, 5005–5017.

T. Árnadóttir, F. Sigmundsson, and E. Sturkell, Nordic Volcanological Center, Institute of Earth Sciences, Natural Sciences Building, University of Iceland, IS-101 Reykjavík, Iceland. (thora1@hi.is; fs@hi.is; sturkell@hi.is)

P. Einarsson, Institute of Earth Sciences, Natural Sciences Building, University of Iceland, IS-101 Reykjavík, Iceland. (palli@raunvis.hi.is)

H. Geirsson, Icelandic Meteorological Office, Bústadavegur 9, IS-150 Reykjavík, Iceland. (dori@vedur.is; ragnar@ vedur.is)

W. Jiang, GPS Research Center, Wuhan University, 129 Luoyu Road, Wuhan, Hubei 430079, China. (wpjiang@whu.edu.cn)

R. Stefánsson, Faculty of Natural Resource Science, University of Akureyri, Sólborg, Norduralód, IS-600 Akureyri, Iceland. (raha@simnet.is)

T. Villemin, LGCA, Université de Savoie, Campus scientifique, F-73376 Le Bourget du Lac Cedex, France. (thierry.villemin@univ-savoie.fr)

C. Völksen, Bavarian Academy of Sciences and Humanities, Marstallplatz 8, D-80539 Munich, Germany. (voelksen@bek.badw-muenchen.de)